CHARACTERISTIC BEHAVIOR OF CROSS-ANISOTROPIC DEPOSITS OF GRANULAR MATERIALS

by

Siddharath Singh

A Thesis
Submitted to the
Graduate Faculty
of
George Mason University
in Partial Fulfillment of
The Requirements for the Degree
of
Master of Science
Civil, Environmental, and Infrastructure Engineering

Committee:

_____	Dr. Burak F. Tanyu, Thesis Director
_____	Dr. Poul V. Lade, Committee Member
_____	Dr. Kuo Tian, Committee Member
_____	Dr. Sam Salem, Department Chair
_____	Dr. Kenneth S. Ball, Dean, Volgenau School of Engineering
Date:_____	Spring Semester 2019 George Mason University Fairfax, VA

Characteristic Behavior of Cross-Anisotropic Deposits of Granular Materials

A Thesis submitted in partial fulfillment of the requirements for the degree of Master of Science at George Mason University

by

Siddharath Singh
Bachelor of Science
George Mason University, 2015

Director: Burak F. Tanyu, Professor
Civil, Environmental, and Infrastructure Engineering

Spring Semester 2019
George Mason University
Fairfax, VA

DEDICATION

This is dedicated to my mom, Foonghua and my dad, Inderpal who supported me through my toughest times in completing this research and to my brother Rohan who pushed me whenever I needed it the most.

ACKNOWLEDGEMENTS

I would like to thank and express my gratitude to my advisor Dr. Burak F. Tanyu and my co-advisor Dr. Poul V. Lade for their guidance and support throughout these three years. I would also like to acknowledge Dr. Saad Ullah, Dr. Aiyoub Abbaspour, Dr. Kuo Tian, Mr. Emre Akmaz, Mr. Andres Cruz, Ms. Binte Zainab, Mr. Inderpal Singh and Mrs. Foonghua Singh for providing valuable support and assistance in this research. I also appreciated the time and feedback from my committee members.

TABLE OF CONTENTS

LIST OF TABLES

LIST OF FIGURES

LIST OF EQUATIONS

LIST OF ABBREVIATIONS AND SYMBOLS

Major Principal Stress ..... σ_1
Minor Principal Stress ..... σ_3
Obliquity ..... σ_1/σ_3
Major Principal Stress – Minor Principal Stress ..... $\sigma_1 - \sigma_3$
Maximum Void Ratio ..... e_{max}
Minimum Void Ratio ..... e_{min}
Diameter of Particle at 10% ..... D_{10}
Diameter of Particle at 30% ..... D_{30}
Diameter of Particle at 60% ..... D_{60}
Coefficient of Uniformity ..... C_u
Coefficient of Gradation ..... C_c
Carbon Dioxide ..... CO_2
Kilo-Pascals ..... kPa
Pounds per Square Inch ..... psi
Skempton's B-Coefficient ..... B-Value
Volumetric Strain ..... ε_v (%)
Original Volume ..... V_O
Volumetric Strain ..... $\Delta V/V_O$
Axial Strain ..... ε_1 (%)
Friction Angle ..... Φ
Dilation Angle ..... ψ
Young's Modulus ..... E
Poisson's Ratio ..... ν
First Stress Invariant ..... I_1
Second Stress Deviator Invariant ..... J_2'
Constant R Function of Poisson's Ratio ..... R
Atmosphere Pressure ..... p_a
Elastic Exponent ..... λ
Elastic Component ..... M
Young's Modulus ..... E
Centimeters ..... cm
Inches ..... in
Celsius ..... °C
Pounds ..... lbs
Milliliters ..... ml
Displacement Transducer ..... DCDT
Different Volume Readings ..... V_n

ABSTRACT

CHARACTERISTIC BEHAVIOR OF CROSS-ANISOTROPIC DEPOSITS OF GRANULAR MATERIALS

Siddharath Singh, M.S.

George Mason University, 2019

Thesis Director: Dr. Burak F. Tanyu

Two series of triaxial compression tests were performed on vertical and horizontal specimens of sand to simulate the cross-anisotropic behavior of soil layers deposited by vertical gravitation in the field. Specimens with horizontal and with vertical bedding planes were created in cylindrical molds and tested in conventional triaxial compression tests. The specimens were pluviated in the vertical direction into an upright mold to create vertical specimens and into the two halves of the mold lying horizontally to create horizontal specimens. The latter were water saturated and frozen and the two halves were assembled to create a cylindrical specimen for testing. These specimens were isotropically confined at 20, 60, and 180 kPa and tested to reveal the behavior of the cross-anisotropic deposit. The characteristic behavior was controlled by the contact normals between the grains which favor the vertical direction, and the stress-strain, volume change, shear strength and elastic properties were analyzed to determine the influence of cross-anisotropy. The behavior of the vertical specimens showed stiffer

initial slopes, smaller strain-to-failure, higher shear strengths and friction angles, less initial contraction and higher rates of dilation than the horizontal specimens. Cross-anisotropy was most pronounced for dense sand and it reduces with increasing confining pressure and increasing void ratio and vanishes at very high confining pressures and high void ratios. The elastic properties evaluated from unloading-reloading cycles showed slightly higher values of Young's moduli for vertical specimens than for horizontal specimens and they increased with the sand density.

1. INTRODUCTION:

Many natural and man-made soil deposits exhibit some degree of cross-anisotropy which is indicated by the material response when loaded in different directions. Granular materials exhibit two types of cross-anisotropy: one is inherent cross-anisotropy in which the particle assembly is in its virgin state before any loading occurs and the other is a result of loading and plastic deformation in one particular direction.

Different studies have been conducted of the characteristics of cross-anisotropy, but few have tested granular material behavior under different loading directions. Rodriguez and Lade (2013) performed torsion shear tests on sand with different stress conditions, as expressed by $b = (\sigma_2-\sigma_3)/(\sigma_1-\sigma_3)$, and different major principal stress directions. They found that it was possible to characterize the three-dimensional failure conditions based on triaxial compression tests on vertical and horizontal specimens, i.e. specimens with horizontal bedding planes in vertical and horizontal specimens, as indicated in Figure 1. In this study, the creation of cylindrical specimens with bedding planes in vertical and horizontal directions is explained, and effects of void ratio and confining pressure on the degree of cross-anisotropy are investigated.

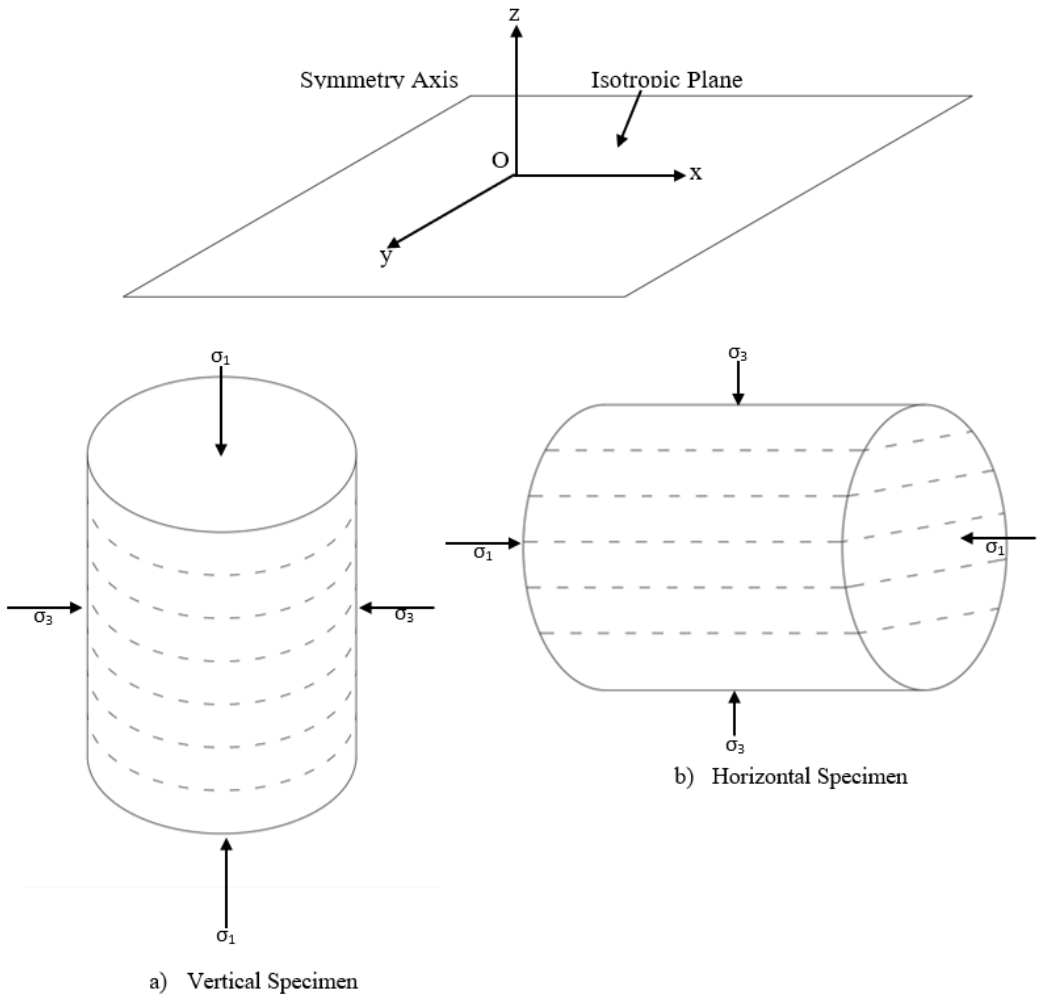

Figure 1. Specimen orientation in cross-anisotropic soil with horizontal bedding planes.

2. PREVIOUS STUDIES OF CROSS-ANISTROPY IN SOILS:

Figure 2a shows a schematic assembly of grains deposited by pluviation through air or water, i.e. gravity causes the grains to move in the vertical direction, and they tend to settle with their long axes in the horizontal direction and with contact angles favoring the vertical direction, as studied by Ochiai and Lade (1983). When this assembly is loaded, and crushing does not occur, the grains have to slide to the side to pass each other. The friction between grains results in stiffer response in the vertical than in the horizontal direction. Because the contact angles tend to be directed in the vertical direction, vertical loading results in smaller deformation and stiffer response than horizontal loading, as indicated in Figure 2b and Figure 2c. Thus, it is the contact angle directions that control the behavior of the granular materials.

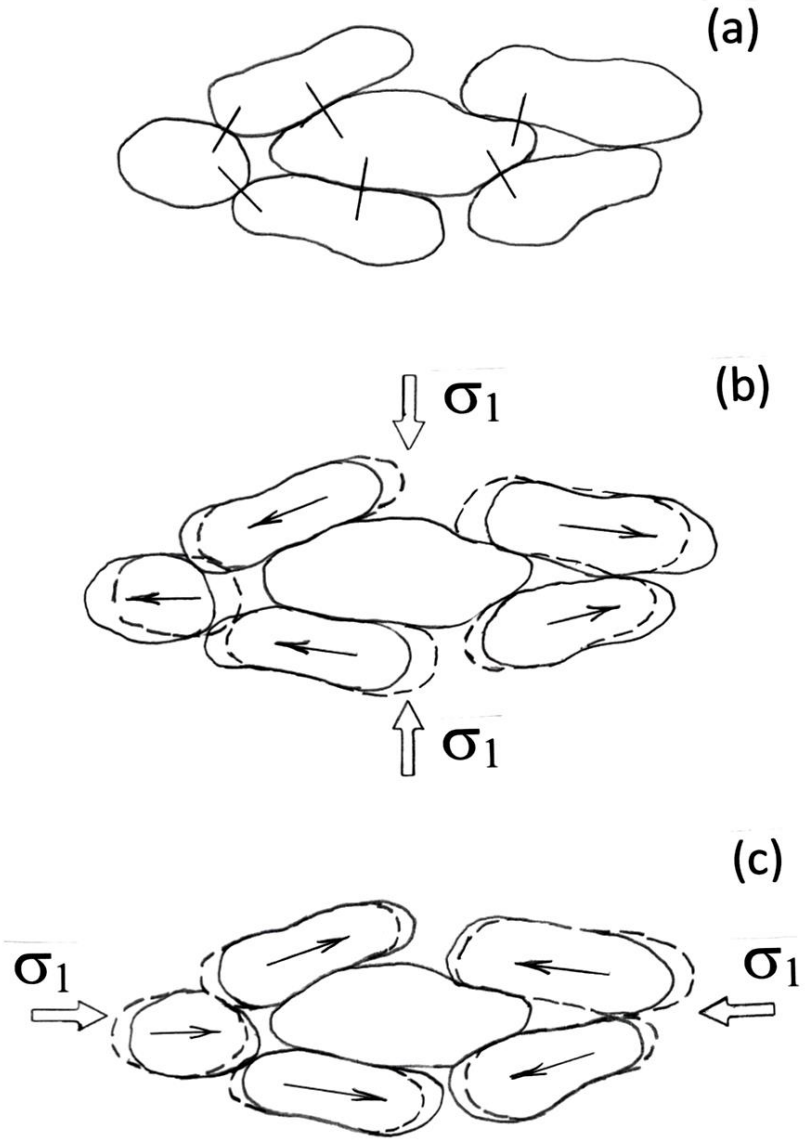

Figure 2. (a) Pluviated sand deposit with contact normals favoring the vertical direction, (b) deposit in the vertical direction, and (c) deposit loaded in the horizontal direction.

The fabric anisotropy of sand deposits may be characterized when the sand particles are relatively large and visible to the naked eye. A number of studies were performed in the late 1960s and early 1970s of the fabric characteristics of random assemblies of 2D and 3D particles as well as natural sands. Parkin et al. (1968), Arthur and Menzies (1972), Arthur and Phillips (1975); Oda (1972a, b, c), and El-Sohby and Andrawes (1973) systematically studied the anisotropic nature of granular materials. It was found that when natural sands or even perfectly round spheres were deposited under force of gravity, the material structure results in a cross-anisotropic fabric. The major reason for this structural anisotropy was found to be a preferred distribution of interparticle contacts that favored the direction of deposition.

The interparticle contact normals are not so easy to determine, but the sand fabric may alternatively be characterized by other measures, such as the preferred orientation of particle long axes. This was done for sands sedimented through both air and water (Oda et al. 1978). The cross-anisotropic sand structure in a pluviated specimen was studied and analyzed in detail in view of the sand grain shapes and their structure by Ochiai and Lade (1983). An indication of the importance of cross-anisotropy in granular materials may be obtained from the laboratory experiments performed by Oda et al. (1978), who compared the bearing capacity of two model strip foundations on sand at different relative densities: one loaded parallel to the sedimentation direction and one normal to it. The resulting values of bearing capacity were different by 50% for the dense sand.

Studies of cross-anisotropy as influenced by the sand fabric were initially performed in triaxial compression on specimens in which the sand was deposited with bedding

planes inclined at different angles, α, of the specimen from 0° to 90° to the vertical axis. These studies (Oda 1972a and b, 1981; Oda et al. 1978; Tatsuoka et al. 1986; Lade and Wasif 1988) indicated that the maximum strength was mobilized when the major principal stress was applied perpendicular to the bedding planes with a transition to lower strengths observed when the major principal stress was aligned with the bedding planes. While these tests were all performed with $b = 0.0$, cross-anisotropy has also been studied in true triaxial equipment to investigate the effects of $b > 0.0$ (e.g. Yamada and Ishihara 1979; Haruyama 1981; Ochiai and Lade 1983; Lam and Tatsuoka 1988; Abelev and Lade 2003, 2004; Lade and Abelev 2003, 2005; Lade et al. 2014a, b). The accumulated evidence shows that under monotonic conditions, when loading and deposition directions coincide, and when no rotation of principal stresses occurs, then the initial anisotropic fabric largely controls the deformation process and the peak shear resistance, especially in sands with elongated particles. This fact has been utilized in testing programs to study the influence of inherent cross-anisotropy on the failure criterion for such soils. The results obtained by Yamada and Ishihara (1979), as well as those obtained by Ochiai and Lade (1983), clearly showed cross-anisotropic stress-strain behavior. However, the failure surfaces observed in these two studies indicated only minor effects and were less clearly influenced by cross-anisotropy.

Only few studies have been performed to find the influence of b and α on the friction angle of sands for various combinations of these two variables. This may be done in directional shear or in torsion shear equipment in which different pressures are applied inside and outside the hollow cylinder specimen. Limited and sporadic experimental

results have been provided in this respect by Arthur and Menzies (1972), Arthur and Philips (1975), Hight et al. (1983), Miura et al. (1986), Pradel et al. (1990), Naughton and O'Kelly (2007), O'Kelly and Naughton (2009) and by Chiaro et al (2013). These studies indicated some variation in friction angle, but none of them provided a complete picture. In comparison, the investigations presented by Lade et al. (2014a, b) showed strong influence of the cross-anisotropic fabric of the granular deposits tested in torsion shear. Rodriguez and Lade (2013) developed a three-dimensional failure criterion for cross-anisotropic deposits for which the parameter values were derived from triaxial compression tests performed on vertical and horizontal specimens. Therefore, it is desirable to investigate the cross-anisotropy characteristics of a granular material under different densities and confinements utilizing the conventional triaxial setup.

3. MATERIAL CHARACTERIZATION:

All tests conducted in this study were performed on "Play" sand obtained commercially from a construction materials store. The geological make-up of the particles was observed to be of silica (quartz) with particle shapes ranging from rounded to sub-angular as determined from Power's Scale of Roundness system (Powers, 1953). The sand was determined to be non-plastic.

Previous literature showed that particles coarser than fine sand will show membrane penetration effects in the volume change measurements when tested in the triaxial cell (Lade, 2016). If ignored, this would create an experimental error since the measured volume change is not representative of the soil skeleton compression, because it includes the volume of water forced out by the penetration of the membrane into the outer layer of sand grains. Therefore, all specimens used in this study were sieved to be within the range of fine sand, i.e. all sand grains coarser than #40 U.S. sieve and finer than #200 U.S. sieve were removed. The particle grain size distribution of the sand used in this study is shown in Figure 3 and properties are summarized in Table 1.

The maximum (e_{max}) and the minimum (e_{min}) void ratios of the fine sand were determined using the procedures described by Lade et al. (1998) by testing each condition with five replicate tests. The results showed consistently that e_{max} and e_{min} values of this sand were 0.90 and 0.57, respectively.

The sand was deposited in specimens with void ratios that ranged from 0.76 to 0.82 for loose, 0.62 to 0.65 for medium dense, and 0.58 to 0.61 for dense conditions. The corresponding relative densities for these void ratios ranged from 24.3% to 41.8% for loose, 73.3% to 82.9% for medium-dense, and 87.7% to 97.3% for dense sand.

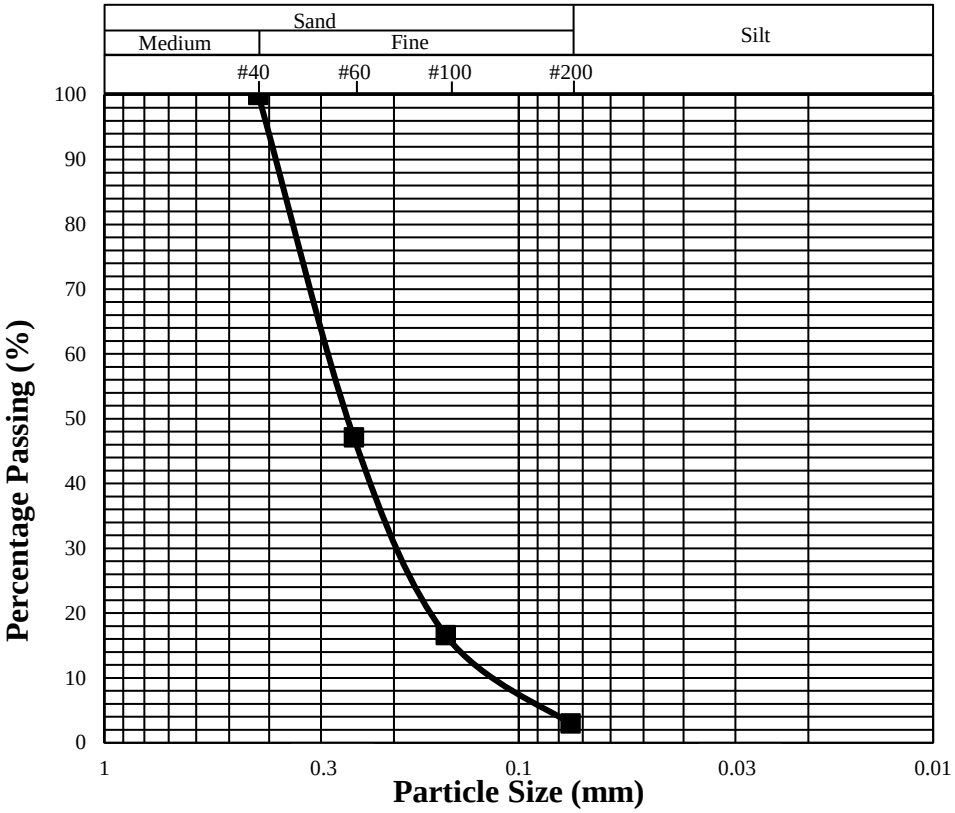

Figure 3. Grain size distribution for Play sand between #40 and #200.

Table 1. Properties of sieved Play sand used in this study

Properties	**Play Sand Values**
D_{10} **(mm)**	0.12
D_{30} **(mm)**	0.20
D_{60} **(mm)**	0.29
C_u	2.42
C_c	1.15
Specific gravity	2.64
USCS classification	SP
Liquid Limit	Non-Plastic
Plastic Limit	Non-Plastic
Maximum void ratio, e_{max}	0.90
Minimum void ratio, e_{min}	0.57

4. SPECIMEN PREPARATION

All tests were conducted in a triaxial chamber with specimen dimensions of 7.1 cm in diameter and with height in the range of 15.5 – 16.0 cm. Specimens prepared at each relative density were tested under three different confining pressures of 20, 60, and 180 kPa. These pressure ranges were selected because previous studies have shown that all properties, including the elastic moduli, change with confining pressure and density (Janbu 1963; Abelev and Lade, 2003). Three of the tests (one at each confining pressure) were conducted by just loading the specimens to failure and beyond, and the other three (one at each confining pressure) were performed by loading, unloading and then reloading the specimens. This protocol was followed because without the loading and unloading, the true Poisson ratio and true elastic moduli values could not be determined (Lade and Nelson, 1987). In addition, results from the tests were compared to evaluate the effects of unloading-reloading rather than just loading of the soil specimens.

All soil specimens were tested vertically under compression loading. However, to evaluate the effects of cross-anisotropy, half of the specimens were prepared vertically, and the other half were prepared horizontally. The following sections describe the preparations of these specimens.

4.1. Vertical Specimens

All specimens were prepared by using a split mold and pluviating the sand into the mold that had a rubber membrane already installed. The targeted void ratios were obtained by raining the sand from different heights (Miura et al. 1982; Vaid et al. 1984b, 1988; Rad and Tumay 1987). To achieve uniform densities within the sand specimen, the rate at which the sand was rained was kept constant. Drop heights of 0 cm, 15.5 cm, and 50 cm were used to create three different densities. The sand was rained through two 7 cm diameter No. 4 U.S. sieves placed on top of a circular cardboard tube. In the case of 0 cm drop, the sand was gently placed over the base of the triaxial chamber using a conical funnel connected to a plastic hose such that the rate at which the sand was released could be controlled at zero drop height. Void ratios were then calculated based on the measured volumes, masses, and specific gravity of the sand.

All of the sand specimens were initially held stable using a vacuum. The vacuum process started after the sand was deposited in the split mold and the top cap was placed. Before removal of the split mold, the valves of the top cap were shut off and the vacuum line was connected through the drainage lines of the bottom base. Only a small amount of vacuum is needed to hold the sand specimen in place. In this study, the maximum applied vacuum was 15 kPa otherwise a larger vacuum may densify the specimen.

After assembling the triaxial cell it was filled with water while the specimen was still under vacuum. The vacuum was then slowly reduced while the pressure in the water was increased such that the specimen continuously felt the same effective confining pressure.

To saturate the specimen with water, gaseous carbon dioxide (CO_2) was first introduced from the bottom drainage line. The gaseous CO_2 replaced the air inside the sand specimen (Lade and Duncan, 1973), and because air is lighter than CO_2, the air was pushed out through the top drainage line and replaced by the CO_2. This replacement process was conducted for about 15 – 20 minutes. The top drainage line was connected to a bubble chamber, which was used to confirm that the air and the gaseous CO_2 entering the sand specimen from the bottom was pushed out of the specimen from the top. The bubble chamber is a glass bottle partially filled with water through which the air is passed to create bubbles thus indicating the movement of gas through the specimen. During this process, it was important to monitor the applied CO_2 pressure entering the sand specimen to check that the effective confining pressure within the specimen does not reduce from the desired conditions.

Following the gaseous CO_2, de-aired water is introduced through the bottom drainage line to percolate slowly into the sand specimen while leaving the top drainage valves open and allowing the CO_2 to be pushed out. Because the sand specimen is initially saturated with gaseous CO_2, the de-aired water will replace the CO_2. Any small amounts of gaseous CO_2 still present in the specimen will dissolve in the intruding water, because approximately one volume of gaseous CO_2 will dissolve into one volume of water at room temperature. In addition, a small back pressure (20 kPa) was applied to the specimen for a period of time (½ to 1 hour) to help the dissolution while increasing the cell pressure (to 35 kPa) allowing the gas bubbles to dissolve under the back pressure. Skempton's B-value was then checked to measure the degree of saturation of the sand

specimen by closing the drainage line and increasing the confining pressure of the sand specimen by 70 kPa and recording the increase in pore pressure. The target B-values for these conditions were in the order of 0.95 and above.

4.2. Horizontal Specimens

The horizontal sand specimens were pluviated to void ratios similar to those of the vertical specimens. To construct a horizontal specimen, the triaxial cylindrical split mold was separated into two halves. A frame was used to hold the molds stationary while the sand was pluviated into the half-cylinder cavities, as seen in Figure 4a. Semi-circular Styrofoam caps were attached to the molds to form the ends of the specimen. A circular tube was used with a 7 cm #4 U.S. sieve attached to the top and moving horizontally to pluviated the sand, as shown in Figure 4b. All the horizontal specimens were formed by depositing the sand vertically into the split molds at a consistent rate as done previously for the vertical specimens. The sand surface was levelled using a spatula to form a flat surface.

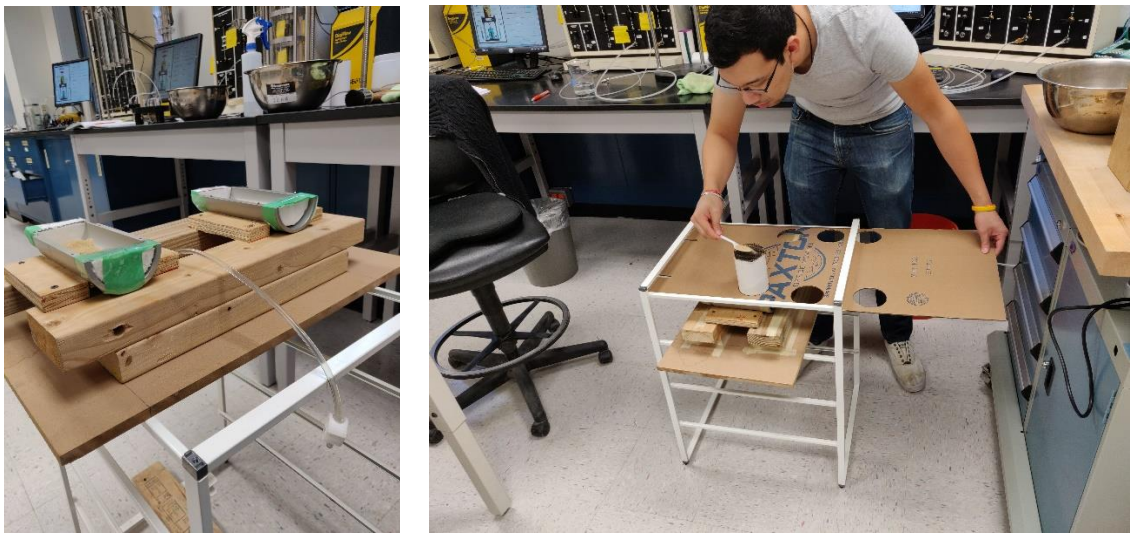

a) **b)**

Figure 4. Preparation of horizontal sand specimens: (a) placement of two molds, and (b) setup used to pluviated sand into split molds.

The half-cylinder specimens were water saturated by introducing de-aired water through the line attached to the sides of the cylindrical split molds. Gaseous CO_2 is not used for this initial saturation procedure. Water saturation is continued until the specimens show dry and wet spots on top of the sand surface, as shown in Figure 5a. Otherwise the subsequent freezing will cause ice to form on top of the sand surface. The wet sand specimens were placed in a freezer for about

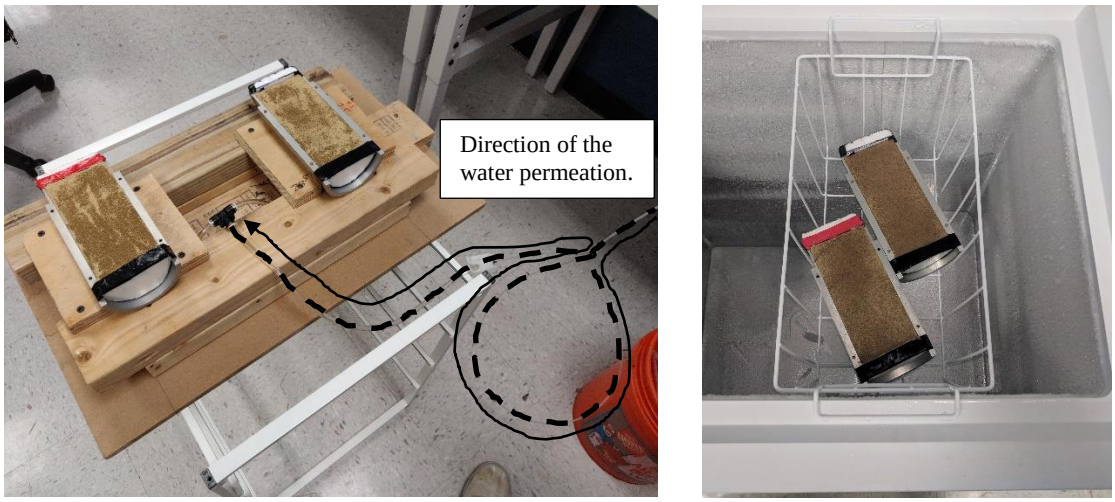

a) **b)**

Figure 5. Horizontal specimens (a) after water permeation up through the sand, and (b) after the specimens are frozen in the freezer.

3 hours, and this allowed the water to freeze throughout, as seen in Figure 5b. Once frozen, the heat from hands was used to warm the exterior of the cylindrical molds sufficiently to melt the water near the interior surface, and then the two half-cylinder specimens were extruded and pressed together to form a cylindrical specimen. Once melted the two halves of the cylinder fit together to form a full cylinder with no visible signs of the formation procedure, as shown in Figure 6.

The frozen horizontal sand specimen was quickly positioned into a rubber membrane and placed on the base of the triaxial chamber. The top cap was attached, and the membrane was sealed to the cap and base. Once the triaxial cell was assembled and filled with water, a cell pressure of 20 kPa was applied. During the process of thawing the

frozen sand specimen, warm water was introduced from the bottom drainage line and percolated through to the top drainage line to help melt the frozen sand specimen.

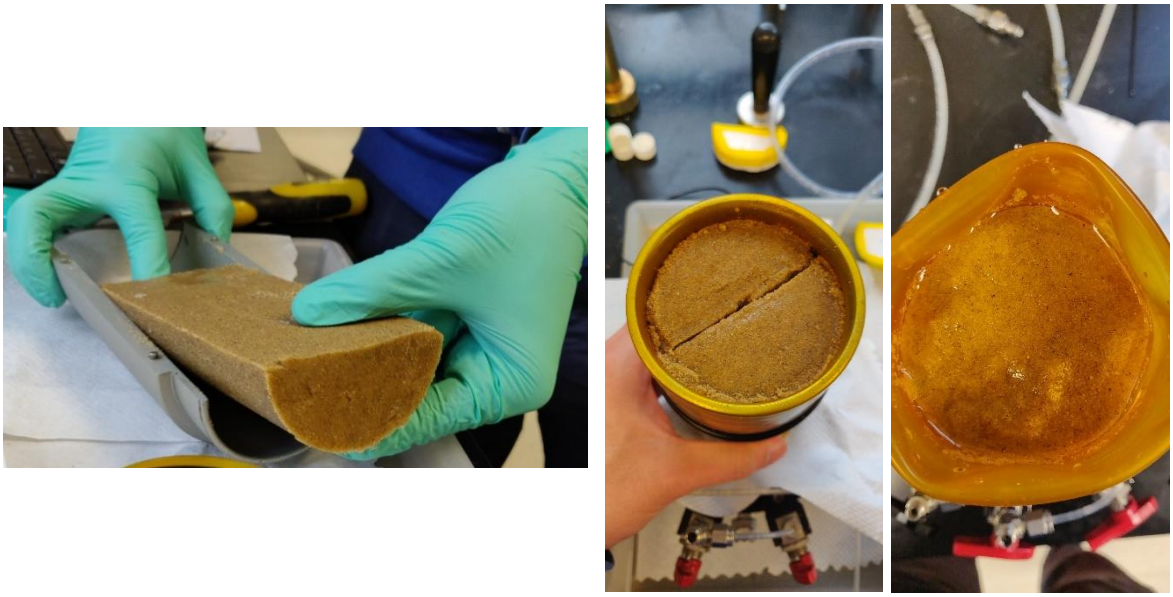

(a) **(b)** **(c)**

Figure 6. Thawing of horizontal specimen after the two halves are joined to create a cylindrical specimen: (a) side views, and (b) top view.

After the sand specimen had thawed, the water in the specimen was removed by a small vacuum of 15 kPa that is applied to the bottom drainage line while the top drainage line was open to allow air to intrude. This air filled the specimen except in the menisci between the grains and, air bubbles were not trapped in these small amounts of water. Gaseous CO_2 was then introduced into the specimen from the bottom drainage line and allowed to seep up through the specimen. This process replaced the air which exiting

through the top drainage line into the bubble chamber, same as was for the vertical specimen saturation procedure where the CO_2 percolated through the specimen for 15-20 minutes. It has previously been observed that the CO_2 method works best when the specimen is initially dry (Lade, 2016), but the results in this study showed that CO_2 method may also be used for the present condition in which the sand particles themselves are slightly wet. Once the horizontal specimen was saturated, the remaining portion of the test proceeded as explained for the vertical specimen.

5. TRIAXIAL COMPRESSION TESTS

Stage 1: Isotropic Compression

The specimens were isotropically compressed to 20, 60, and 180 kPa respectively, before the triaxial compression tests were performed at these three constant confining pressures. The results of isotropic compression of vertical and horizontal specimens of medium dense sand up to 60 and 180 kPa are shown in Figure 7.

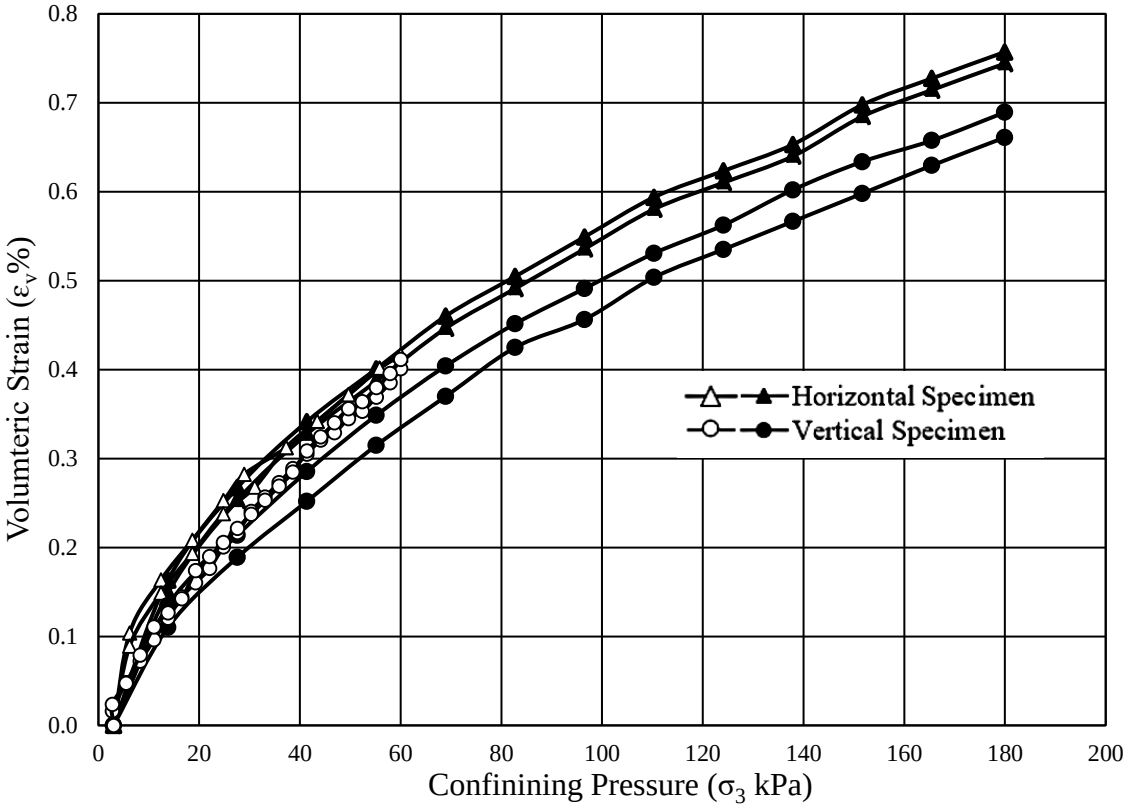

Figure 7. Volumetric strains of vertical and horizontal medium dense specimens for isotropic compression up to 60 kPa and 180 kPa.

While the two types of specimens are expected to show the same isotropic compression curves, the horizontal specimens indicate slightly larger volumetric compression than the vertical specimens. However, the difference is within the experimental scatter of such tests. Similar results were obtained for loose and dense sand specimens.

Stage 2: Shearing

The shearing stage of the tests on both vertical and horizontal specimens were conducted with an axial strain rate of 10%/hr up to a maximum strain of 20%. To

produce results from which the elastic moduli could be determined, half of the triaxial compression tests were sheared to just beyond smooth peak failure after which an unloading-reloading cycle was included. The sand specimens were consequently unloaded at an axial strain of approximately 6%. At this point the fabric of the specimens has changed minimally and the elastic moduli are therefore expected to be representative of the void ratios of the respective specimens.

6. STRESS-STRAIN BEHAVIOR

The stress-strain and volume change curves from the triaxial compression tests are presented in Figure 8. The stress-strain and volume change behavior shown in Figure 8a shows the vertical and the horizontal medium dense sand specimens loaded to failure and beyond for all three confining pressures. Figure 8b shows similar results for the specimens that were unloaded and reloaded near smooth peak failure.

The shapes of the stress-strain curves for the vertical and horizontal specimens are very different as peak failure is approached. This is due to the grain configuration in the vertical and horizontal specimens. It takes larger strains to mobilize the full shear strength in the horizontal than in the vertical specimens.

As shown by the stress-strain behavior in Figure 8, the mobilization of shear strength requires larger strains for the horizontal than for the vertical specimens. This is because the grains are pushed together at lower slopes and the resistance to compression and movement of grains are lower for the horizontal specimens than for the vertical specimens.

6.1. Initial Slopes

The initial slopes shown in Figure 8 for the vertical specimens are consistently stiffer than those for horizontal specimens. This is due to the grain structure in the cross-anisotropic deposits, which may be characterized by contact normals that favor the

vertical direction. This provides for stiffer response in the vertical direction than in the horizontal direction as explained in connection with Figure 1. The initial slopes for the horizontal sand specimens do not show a sharp rise similar to those of the vertical sand specimens.

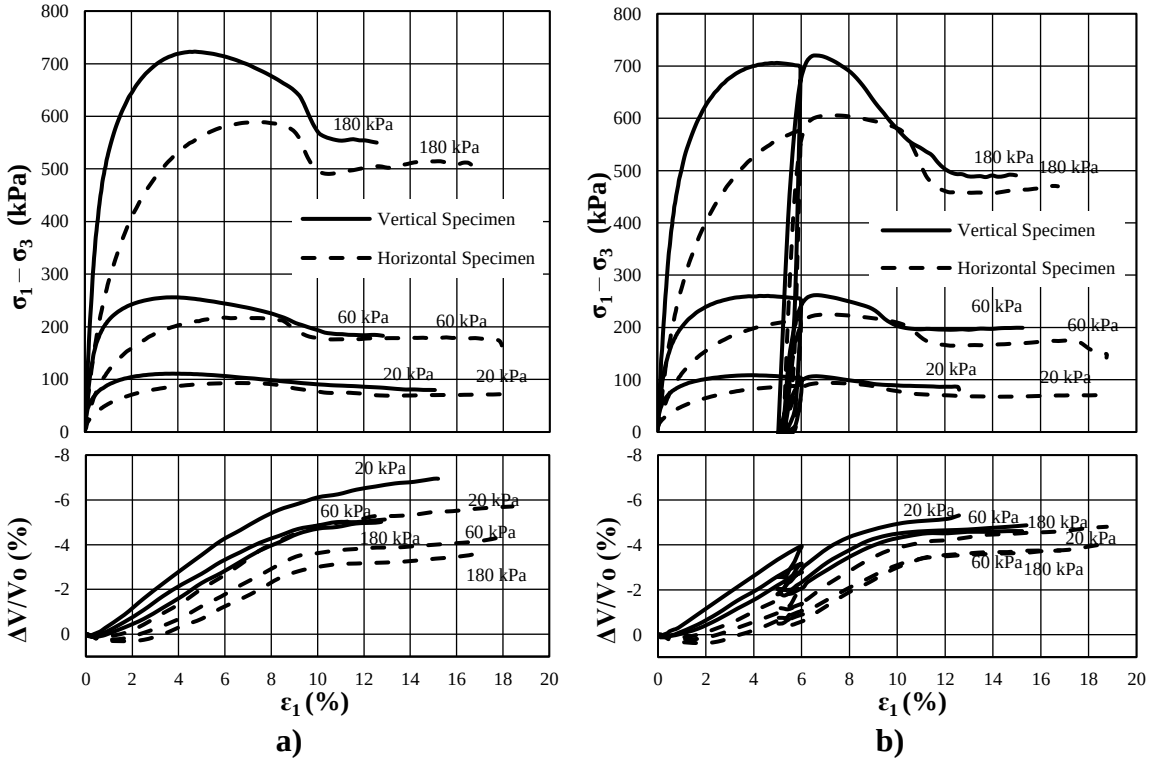

Figure 8. Stress-strain and volume change relations for medium dense vertical and horizontal sand specimens in triaxial compression tests with (a) loaded only, and (b) including unloaded-reloaded cycles.

6.2.Strain-to-Failure

The stress-strain behavior of vertical and horizontal specimens is distinctly different due to the grain structure. Thus, the vertical specimens show a rapid rise and a higher strength than the horizontal specimens, which exhibit much slower increase in shear resistance. The horizontal specimens also reach peak failure after substantially larger amounts of sliding, and consequently, the horizontal specimens reach smooth peak failure at larger values of axial strain than the vertical specimens.

6.3.Shear Strength

The smooth peak failure points for the two specimen types are different and indicate that the vertical specimens have a higher strength than the horizontal specimens. This is also due to the grain structure, which determines their behavior. Inspection of results for dense and loose specimens, which are not shown in this presentation, indicates that this difference increases with increasing density. For loose specimens the difference in strength tends to zero, and the influence of cross-anisotropy is minimal. Cross-anisotropy is therefore most pronounced in dense sand deposits.

Figure 8b shows the behavior of the medium dense sand specimens that include an unloading-reloading cycle for the vertical and horizontal sand specimens. All aspects of the stress-strain behavior up to failure are very similar to those observed for the first series of tests, thus indicating the reproducibility of the tests. During the reloading process both types of sand specimens densify causing the following failure points to increase to slightly higher values.

6.4.Shear Banding

Figure 8 show that shear banding develops in the softening regime in all specimens. Most often much larger axial strains than those reached for peak failure are required for shear banding to occur. This has been observed before and it matches theoretical predictions (Lade 2003). The shear band development is indicated by the break in the stress-strain relations in the softening regime and by the reduction in dilation rate in the volume change curves. While dilation is required for development of shear bands, once they develop, the void ratio inside the shear band becomes larger and the shear strength becomes lower than in the surrounding sand masses. The following sliding consequently occurs along the shear band, which has now exhausted its capacity for dilation, followed by very little or no further dilation in the specimen. This behavior is more pronounced for dense specimens (not shown) than for medium dense sand, as shown in Figures 8, but it is not so prominent for the loose sand (not shown). This is because shear banding requires the sand to dilate and loose sand dilates less vigorously than dense sand or not at all.

Figure 8b shows that the vertical sand specimens that included an unloading-reloading cycle developed shear bands in a similar way to the vertical sand specimens that were just loaded, as indicated in Figure 8a. Note that the vertical specimens in Figure 8b decreased in shear strength until they developed shear bands around an axial strain of 8-9%, very similarly to those without unloading-reloading cycles. The horizontal sand specimens exhibited shear banding at slightly larger axial strains near 9-10%. The trends in the vertical and horizontal specimens were similar whether or not they included an unloading-reloading cycle.

6.5.Volume change

Both Figures 8a and b indicate that the vertical and horizontal specimens of medium dense sand showed increasing initial contraction and decreasing rates of dilation with increasing confining pressure. Further, the horizontal specimens showed more contraction than the vertical specimens and they dilated at a slower rate than the vertical specimens. Similar results were obtained for the vertical and horizontal sand specimens that were unloaded and reloaded, as shown in Figure 8b. However, during reloading, all the specimens initially dilated faster than indicated by the corresponding specimens without unloading-reloading.

6.6.Friction angles

The friction angles were calculated using the maximum obliquity, σ_1/σ_3, measured during testing of the sand specimens:

Equation 1. Friction angle calculated using the maximum obliquity.

$$\Phi = \arcsin\frac{\sigma_1 - \sigma_3}{\sigma_1 + \sigma_3} = \arcsin\frac{\frac{\sigma_1}{\sigma_3} - 1}{\frac{\sigma_1}{\sigma_3} + 1}$$

Table 2 gives the friction angles of all sand specimens that were (1) loaded only, and (2) unloaded and reloaded in the vertical and horizontal directions. It is observed that inherent cross anisotropy results in significantly higher friction angle in vertical than in horizontal specimens.

Table 2. Summary of friction and dilation angles for vertical and horizontal sand specimens.

Table 2. Summary of friction and dilation angles for vertical and horizontal sand specimens.

	Loaded Only						Unloaded and Reloaded					
	20 kPa	60 kPa	180 kPa	20 kPa	60 kPa	180 kPa	20 kPa	60 kPa	180 kPa	20 kPa	60 kPa	180 kPa
Friction Angle	**Vertical**			**Horizontal**			**Vertical**			**Horizontal**		
Dense	48.6	44.8	43.2	43.4	41.1	39.5	48.4	44.8	42.7	44.7	42.1	40.4
				42.3	41.4	39.7				44.7	41.7	40.6
Medium dense	46.1	42.9	41.8	43.4	39.8	38.3	46.1	42.8	41.7	42.6	40.4	38.8
Loose	39.3	37.5	35.5	37.9	35.7	34.7	40.3	37.2	35.6	37.9	36.6	34.7
	38.3	37.2	35.5				40.2	37.8	35.7			
Dilation Angle												
Dense	19.3	17.3	15.9	15.8	15.3	13.9	19.3	16.8	15.8	17.3	17.2	15.3
				15.3	15.6	14.2				17.6	16.3	15.7
Medium dense	16.7	14.7	13.8	13.7	12.6	12.3	16.5	14.6	14.0	14.0	13.5	13.3
Loose	4.9	5.0	4.3	5.6	6.4	6.2	6.7	6.7	5.0	7.7	8.1	6.6
	4.1	5.0	4.2				7.6	8.2	5.4			
Difference Between Friction and Dilation Angles												
Dense	29.3	27.5	27.3	27.6	25.9	25.6	29.1	28.0	27.0	27.5	25.0	25.1
				27.0	25.8	25.6				27.1	25.4	24.9
Medium dense	29.5	28.3	28.0	29.7	27.2	26.0	29.5	28.3	27.7	28.6	26.9	25.5
Loose	34.4	32.5	31.2	32.3	29.3	28.5	33.6	30.4	30.6	30.2	28.5	28.1
	34.2	32.3	31.4				32.7	29.6	30.2			

Figure 9 shows the variation of friction angles with confining pressure for dense and loose specimens that were loaded only (Figure 9a) and unloaded and reloaded (Figure 9b). The values for the medium dense sand were not added to this figure for clarity, however, can be obtained from Table 2. The friction angles in all cases decrease with increasing confining pressure as previously found for sands (Lee and Seed 1967). They also show that vertical specimens have higher friction angles than the horizontal specimens. Further, the loose specimens show smaller differences between the horizontal

and vertical specimens than the dense specimens. Thus, cross-anisotropy is most pronounced for dense sand. A second series of loose vertical and dense horizontal sand specimens were used to indicate the repeatability of the experimental results, as shown by the very similar friction angles.

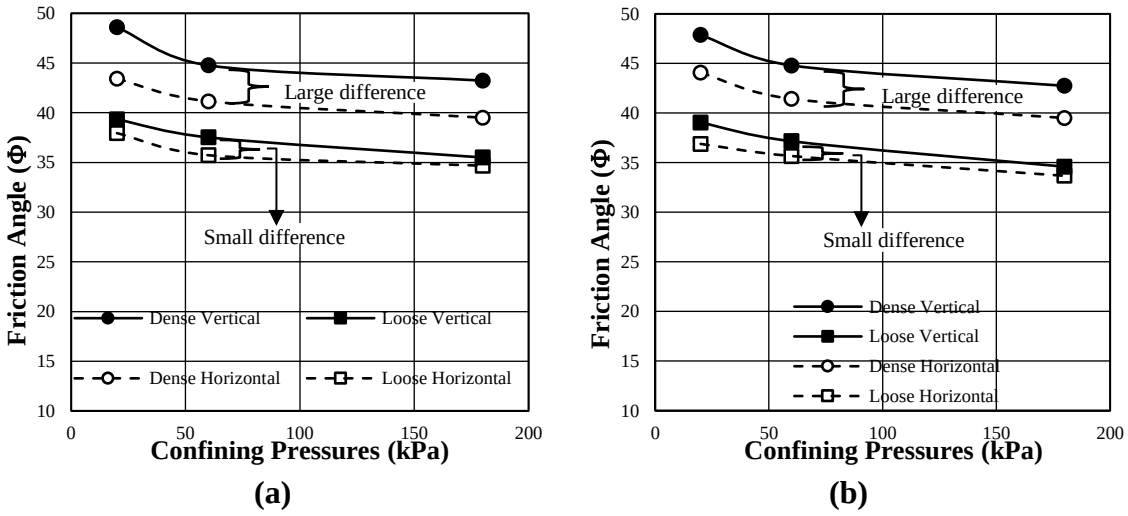

Figure 9. Variation of friction angles for medium dense vertical and horizontal sand with confining pressure. (a) Loaded only and (b) unloaded and reloaded.

6.7.Dilation angle

The dilation angle is determined from the tangent of the volumetric strain versus the axial strain curve measured at peak failure in the triaxial compression tests:

Equation 2. Dilation angle from the tangent of the volumetric strain vs the axial strain.

$$\psi = \arcsin\left(\frac{\frac{d\varepsilon_v}{d\varepsilon_a}}{\frac{d\varepsilon_v}{d\varepsilon_a} - 2}\right)$$

Table 2 also shows the dilation angles for the sand specimens. They have a similar trend as the friction angles where the dilation angles for the vertical specimens being larger than the dilation angles for the horizontal specimens.

Inherent cross anisotropy influences the dilation angles for the sand specimens deposited in two different directions. Thus, the dilation angles are smaller for the horizontal than the vertical specimens. Figure 10 shows the difference between the friction angles and the dilation angles ($\phi - \psi$) for the vertical (solid lines) and the horizontal specimens (dashed lines) plotted versus the

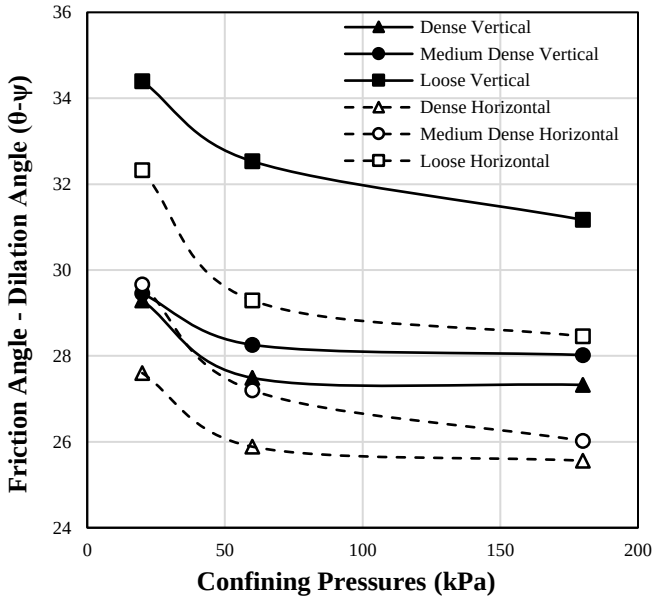

Figure 10. Difference between friction and dilation angles for medium dense and horizontal sand with confining pressures.

confining pressure. All experiments show that the differences between the friction angles and the dilation angles ($\phi - \psi$) decrease as the confining pressure increases. However, the differences between friction angles and corresponding dilation angles decrease as the density of the sand specimen increases. The loose sand specimens in both the vertical and horizontal directions have higher values than the medium dense and the dense sand specimens. Similar tests were conducted on vertical specimens by Lee and Seed (1967) on loose, medium loose, medium dense and dense Sacramento River sand and their results show behavior comparable to that observed in the present experiments.

6.8.Elastic Properties

To evaluate the elastic properties of the sand specimens, the slopes of the stress-strain and volume change relations during unloading and reloading were evaluated (Lade and Nelson 1987, Lade 2016). The Young's moduli are determined immediately after stress reversals, such that no plastic strains are involved in the evaluation. Thus, Equation 3 is employed to calculate Young's modulus (E) from axisymmetric loading conditions. Figure 11a shows a schematic diagram in which two values of Young's modulus are determined from the points of unloading and reloading. In both cases, these moduli are associated with the stress points where stress reversal takes place. Poisson's ratio (ν) is determined from the slope of the volumetric strain versus the axial strain curve when the specimen is being reloaded as shown schematically in Figure 11b. Poisson's ratio is then calculated using Equation 4.

Equation 3 Young's modulus from axisymmetric loading conditions.

$$E = \frac{\Delta(\sigma_1 - \sigma_3)}{\Delta\varepsilon_1}$$

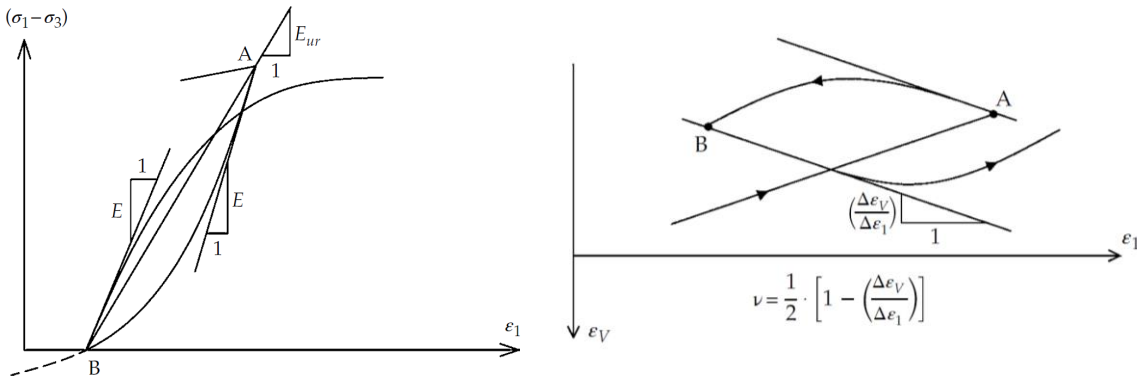

(a) **(b)**

Figure 11. Schematic diagrams of determination of (a) elastic moduli at stress reversal points, and (b) Poisson's ratio from volume change relations during reloading of triaxial specimens. (Lade, 2016)

Equation 4. Poisson's ratio formulation

$$v = \frac{1}{2}\left(1 - \frac{\Delta\varepsilon_v}{\Delta\varepsilon_1}\right)$$

To model the elastic strains, a nonlinear variation of Young's modulus with the state of stress was developed by Lade and Nelson (1987). This model was developed on the basis of a constant Poisson's ratio, as it is most often found to be from experimental evidence. The Young's modulus is expressed in terms of stress invariants, as given in Eq. 5:

Equation 5. Young's modulus with the state of stress.

$$E = M * p_a \left[\left(\frac{I_1}{p_a}\right)^2 + R * \frac{J_2'}{p_a^2}\right]^{\lambda}$$

Equation 6. First stress invariant calculation.

$$I_1 = \sigma_1 + \sigma_2 + \sigma_3$$

Equation 7. Second stress invariant calculation.

$$\mathbf{J_2' = \frac{1}{6}[(\sigma_1 - \sigma_2)^2 + (\sigma_2 - \sigma_3)^2 + (\sigma_3 - \sigma_1)^2]}$$

Equation 8. R parameter function of Poisson's ratio

$$R = 6 * \frac{1+\nu}{1-2\nu}$$

In Equation 5 the values of M and λ are non-dimensional parameters and p_a is the atmospheric pressure in the same units as used for calculation of the stress invariants I_1 and J'_2 given in Equation 6 and 7**,** respectively. The parameter R is a function of Poisson's ratio as given in Equation 8. Parameters M, λ and ν are the three material parameters that are required to express the elastic behavior. Using Equations 5–8, the material parameters M and λ can be determined by plotting $\left[\left(\frac{I_1}{p_a}\right)^2 + R\left(\frac{J_2'}{p_a^2}\right)\right]$ versus (E/p_a) in a log-log diagram. Figure 12 shows the determination of the values of M and λ for the vertical and horizontal medium dense specimens.

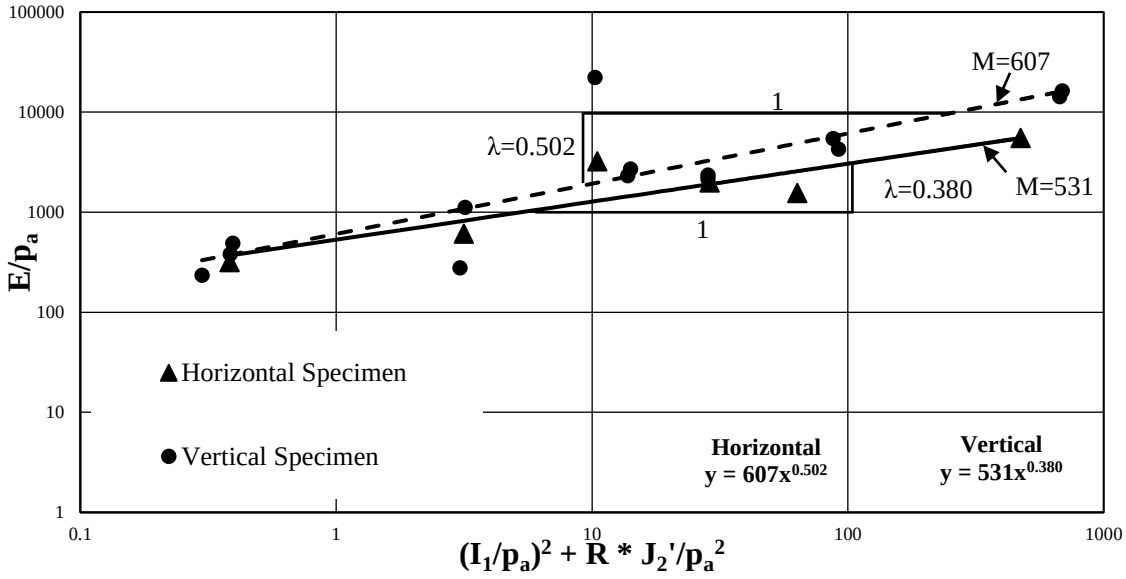

Figure 12. Determination of parameters M and λ for characterization of elastic modulus variation for medium dense vertical and horizontal sand with changes in stress state.

All elastic material parameters are given in Table 3 for the vertical and horizontal sand specimens of loose, medium dense and dense sand. The vertical specimens have slightly higher values of M for all densities than the horizontal specimens. A slight tendency for larger values occurs with increasing density.

Table 3. Summary of all test results for the calculated elastic properties of the vertical and horizontal specimens.

Void Ratio	0.79	0.79	0.80	0.65	0.65	0.59	0.60	0.60
Density	Vertical Loose Set-1	Vertical Loose Set-2	Horizontal Loose	Vertical Medium Dense	Horizontal Medium Dense	Vertical Dense	Horizontal Dense Set 1	Horizontal Dense Set 2
Elastic Properties:								
ν (Poissons Ratio)	0.46	0.45	0.42	0.38	0.37	0.35	0.34	0.33
M (Elastic Component)	222.51	224.32	258.44	607.24	531.09	675.87	539.25	550.40
λ (Elastic Exponent)	0.49	0.49	0.43	0.50	0.38	0.43	0.43	0.38

7. CONCLUSIONS

A comprehensive experimental investigation was undertaken to study the cross-anisotropy observed in triaxial compression tests on sand specimens deposited into vertical and horizontal specimens. A series of conventional triaxial tests were performed on loose, medium dense and dense air-pluviated specimens of fine Play sand. The sand specimens were tested under three different confining pressures, 20, 60, and 180 kPa and two sets of experiments were performed: one set where the specimens were loaded only and another set with specimens unloaded-reloaded in a cycle. The techniques for creating specimens with horizontal layers of sand in vertical and in horizontal specimens were explained in detail.

The volumetric change during isotropic compression was very similar and within the scatter of experiments for the vertical and horizontal sand specimens. The volumetric strains for loose and dense sand specimens resulted in similar trends as observed for the medium dense sand.

The details of the behavior of cross-anisotropic deposits of sands are explained by the contact angle directions between grains. These directions tend to favor the vertical direction and the consequent stress-strain and volume change characteristics can all be explained in view of the consequent cross-anisotropic behavior. Detailed analyses indicated that (1) the initial slopes of the vertical specimens were higher than those for

horizontal specimens, (2) the strains-to-failure were smaller for the vertical specimens, (3) the shear strengths were higher for the vertical specimens, (4) shear banding occurred well after smooth peak failure in both vertical and horizontal specimens and were not affected by unloading-reloading cycles, (5) the vertical and horizontal specimens of medium dense sand showed increasing initial volumetric contraction and decreasing rates of dilation with increasing confining pressure, (6) the horizontal specimens showed more contraction than the vertical specimens and they dilated at a slower rate than the vertical specimens, (7) the friction angles were higher for vertical than for horizontal specimens and they all decreased with increasing confining pressure, (8) the loose specimens showed smaller differences in friction angles than the dense specimens, (9) the angles of dilation showed similar trends as the friction angles, (10) the differences between the friction angles and the dilation angles were highest for the vertical specimens and they were highest for the loose specimens, (11) the elastic properties evaluated from the unloading-reloading cycles showed slightly higher values of Young's moduli for vertical specimens than for horizontal specimens and increasing with the sand density, and (12) the essentially constant Poisson's ratio decreased with increasing density.

Overall the results showed that conventional triaxial tests on cylindrical specimens can be employed for investigating cross-anisotropy using specimens with bedding planes in horizontal and vertical directions. The overall evaluation of test results is that cross-anisotropy is most pronounced for dense sand and it reduces with increasing confining pressure and increasing void ratio and vanishes at high void ratios.

APPENDIX

Appendix A – Obtaining Maximum and Minimum Void Ratios

Maximum and minimum void ratios are obtained using the methodology given from Lade et. al in "Effects of Non-Plastic Fines on Minimum and Maximum Void Ratios of Sand" (1998). In Figure 1a, the equipment shown on the counter are the items needed to perform the test. A 2000 ml graduated cylinder, a bowl of 1000 grams of sand sieved between passing #40 and retained #200 sieves, spoon, latex membrane cut out in the shape of the top of the graduated cylinder, tape, and rubber pastel or a soft rubber hammer.

Deposit 4 spoonful of sand evenly through air pluviation and then use the end of the rubber pastel and tap the sides of the cylinder lightly 8 times, 2 times in all 4 directions. Keep depositing the sand until you run out of sand in the bowl and record the minimum height of the sand in the graduated cylinder as shown in figures 1b. Attach the latex membrane to the top of the graduated cylinder using the tape and check to see if there are any openings on the top. Hold the cylinder by placing your hands on the top (covering the latex membrane) and the bottom of the cylinder and rotate the cylinder slowly for 1 minute until you have rotated it 180°. Rotate the cylinder slowly until it is back to the original position and record the maximum height as shown in Figure 1d. Repeat the rotation process until the maximum height of the specimen stays constant.

Use the phase diagram to calculate the minimum and maximum void ratios of the given specimens. The minimum height of the specimen will result in a small void ratio whereas the maximum height of the specimen will result in a larger void ratio.

a)

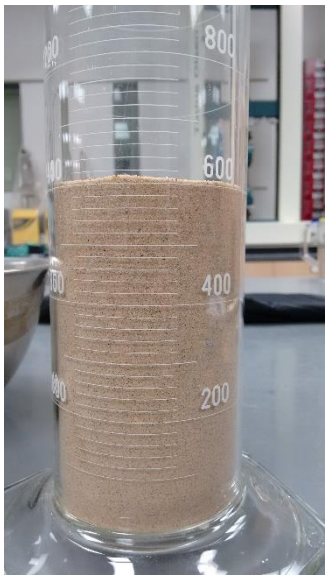

b)

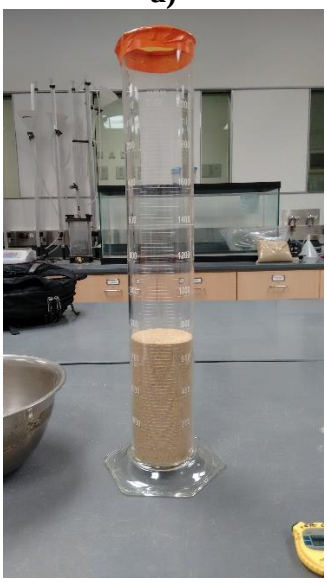

c)

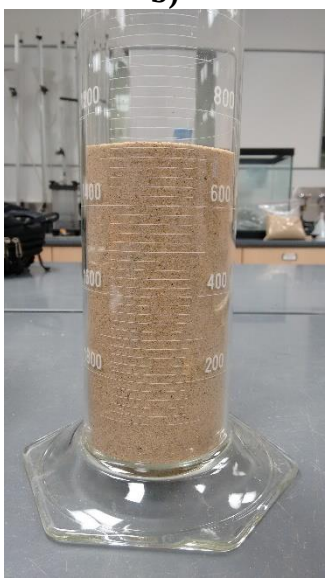

d)

Figure 1. (a) Equipment used for the minimum and maximum void ratio test. (b) Record the minimum height for the minimum void ratio. (c) Equip the latex membrane to the top of the graduated cylinder and tape it. (d) After the specimen is rotated 180°, record the maximum height for maximum void ratio.

Appendix B – Details of Sample Preparations and Associated Calculations

Vertical Specimen:

1. The sand used to create the vertical sand specimens are sieved between the range of passing #40 sieve and retained #200 sieves. Back calculate the targeted void ratio to get the weight of the sand needed for the deposition process of the specimen. The formulation of the mass is the unit weight of specimen multiplied with the volume of the cylindrical split mold as shown in Equation 1.

$$Mass = Mold\ Vol. * \gamma \qquad \textbf{Eq. 1}$$

2. Attach small strips of non-woven geotextiles to the holes of the top and bottom caps within the triaxial chamber. The grade of the non-woven geotextiles should be 200 N as you want to make sure that no sand particle gets through the small holes in the caps as seen in Figure 2.

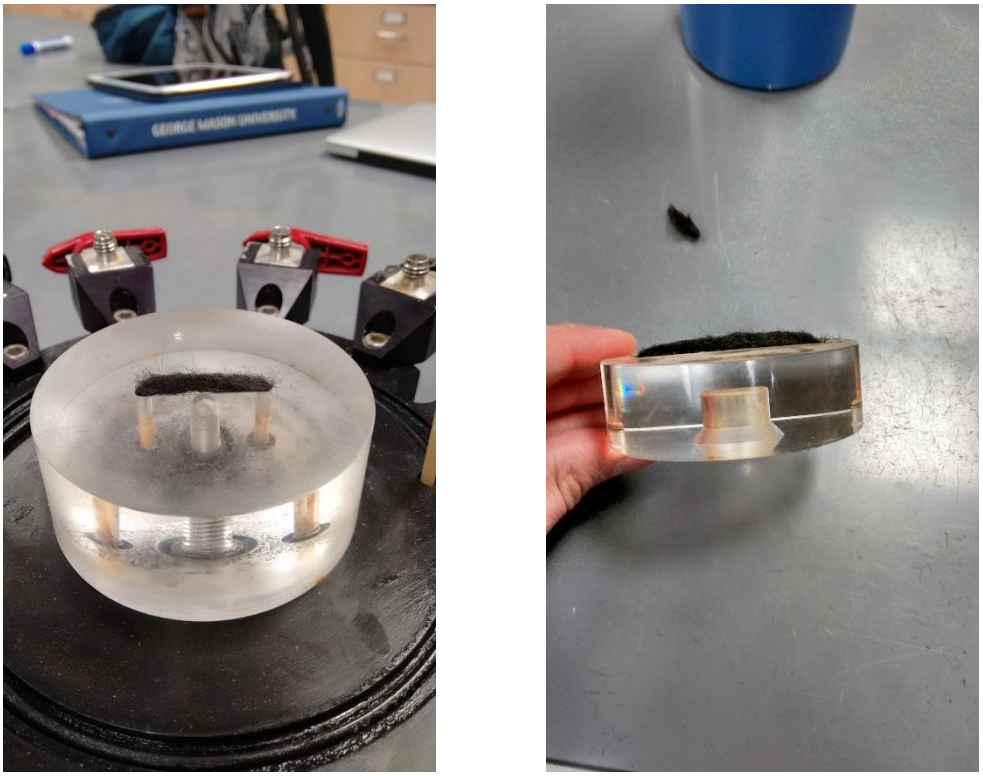

a) **b)**

Figure 2. (a) Non-woven 200N grade geotextile strip is inserted into the small holes in the bottom cap. (b) Non-woven 200N grade geotextile strip in inserted into the small holes of the top cap.

Afterwards, place the latex membrane around the bottom cap and attach the O-rings to the bottom cap. Place the split mold on top of the bottom cap and wrap the latex membrane that is attached to the bottom cap around split mold. Introduce vacuum pressure into the split mold to allow the latex membrane to create a smooth even surface.

3. Deposit the measured sand into the split mold at different heights pertaining to the density that is needed to be reached for the sand specimen. For dense sand specimens, deposit spoonful of sand into the split mold at a height of 50 cm from the bottom cap shown in Figure 3a, for medium-dense sand, deposit sand at a height of 15.5 cm from the bottom cap shown in Figure 3b, and loose sand specimens require a height of 0 cm from the bottom cap shown in Figure 3c.

   Dense sand specimens require a tube attached to the top of the split mold as shown in Figure 3a and attach two small sieves to the top of the tube to evenly distribute the sand. The medium dense sand will require a height of 15.5 cm which is the height of the split mold from the base of the bottom cap all the way to the top of the split mold. Use a smooth paper cylindrical tube inside the split mold and lift the cylinder after every 4 cm. Place a small sieve (gutter screen) on the top to evenly distribute the sand in the mold. For loose sand specimens attach a tube to a funnel to distribute the sand very close to the surface of the bottom cap as shown in Figure 3c.

4. Place the top cap inserted with geotextiles on top of the sand specimen and fold the latex membrane over the top cap allowing the latex membrane to encapsulate the top cap and the specimen. Attach the O-rings to the top cap covered by the latex membrane and insert the water lines into the holes in the top cap. Turn off the vacuum pressure on the split mold and leave the split mold in place. Move to Appendix C.

a) **b)** **c)**

Figure 3. (a) Dense sand specimen at a height of 50 cm, (b) medium dense sand specimen at 15.5 cm, (c) loose sand specimen with funnel and tube used close to the surface of bottom cap.

Horizontal Specimen:

1. Follow the first step of creating the vertical sand specimen by measuring the amount of sand needed to create a dense, medium-dense or loose specimen. Perform this step by using the same void ratios used in the vertical sand specimens and back calculating those void ratios to measure the weight of sand needed for the horizontal sand specimens. This is to have equal void ratios for the vertical and horizontal specimens during the triaxial test. Insert the 200N grade nonwoven geotextiles strips into the bottom cap and top cap of the triaxial cell.

2. Split the molds into halves and insert semicircular Styrofoam caps into the mold as shown in Figure 4. Insert a small strip of geotextile 200 N grade into the center hole, this is to stop sand from clogging the vacuum lines. Place the split molds on top of a frame to hold the split molds stationary and attach the vacuum lines into the split molds to allow access to water.

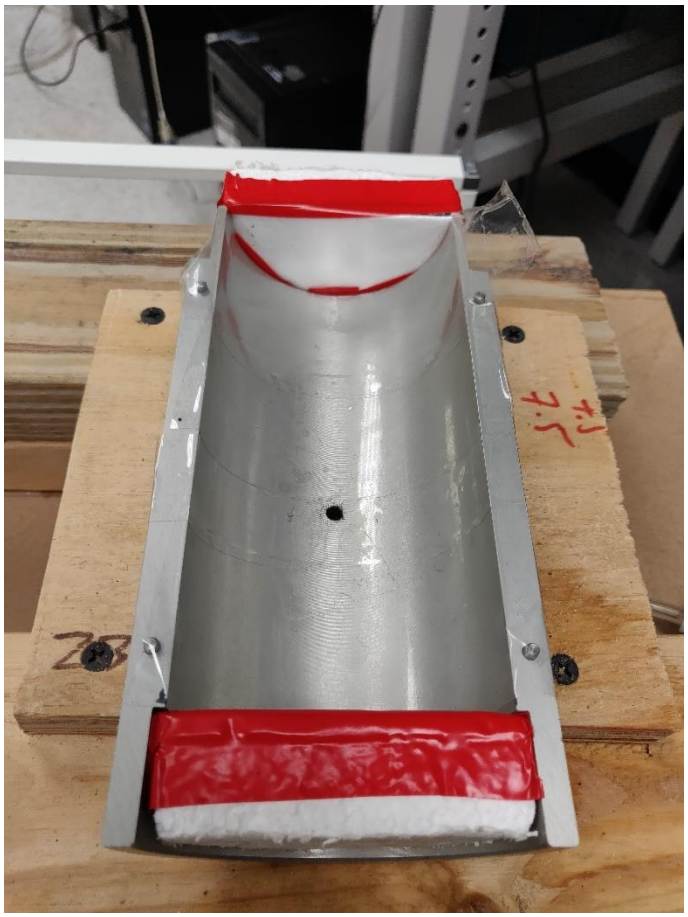

Figure 4. Place the semi-circular Styrofoam cap inside the concave opening of the split mold and attach the other Styrofoam cap to the sides of the top part of the split mold. Use tape to secure their positions. The split mold is held on top of the frame.

A cardboard cutout is taken and placed in the top shelf with a smooth tube inserted into the cutout to allow the tube to move backwards and forwards while depositing the sand. The frame holding the split molds is placed directly underneath the cardboard cutout which is on the second shelf. Dense sand specimens will be produced at a height of 50 cm from the base of the split mold

when laid horizontally while medium-dense sand samples are produced at a height of 15.5 cm from the base of the split mold laid horizontally as shown in Figure 5a. Push and pull the cardboard cutout holding the tube while depositing spoonful of sand into the split mold with the sieve screen attached on the top of the tube.

For loose sand specimens, remove the cardboard cutout from the top shelf and place the frame holding the split molds on the top shelf. Deposit spoonful of sand very close to the base of the split molds while moving the spoon from one Styrofoam cap to the other to create the horizontal loose specimen as shown in Figure 5b.

a) **b)**

Figure 5. (a) The frame is kept on the second shelf with the cardboard cutout inserted in the top shelf which is then allowed to move while depositing sand for both the dense and medium-dense sand specimens. (b) The sand is placed in the same direction as figure 5a however the sand is deposited close to the surface.

3. Saturate the sand specimens using the vacuum lines attached to the split molds shown in Figure 6a. Use the deaired water through the deaired water panels and attach the water line to the vacuum line and allow the water to flow without any added back pressure. Saturate the sand specimen before it is completely saturated as shown in Figure 6b otherwise the specimen will form ice mounds on top of the sand specimen if it is oversaturated. Remove the vacuum lines once they have saturated the specimen and place the split molds in the freezer and turn the freezer knob to 3.5. Keep the sand specimen in the freezer for 3 hours to allow the specimen to completely freeze.

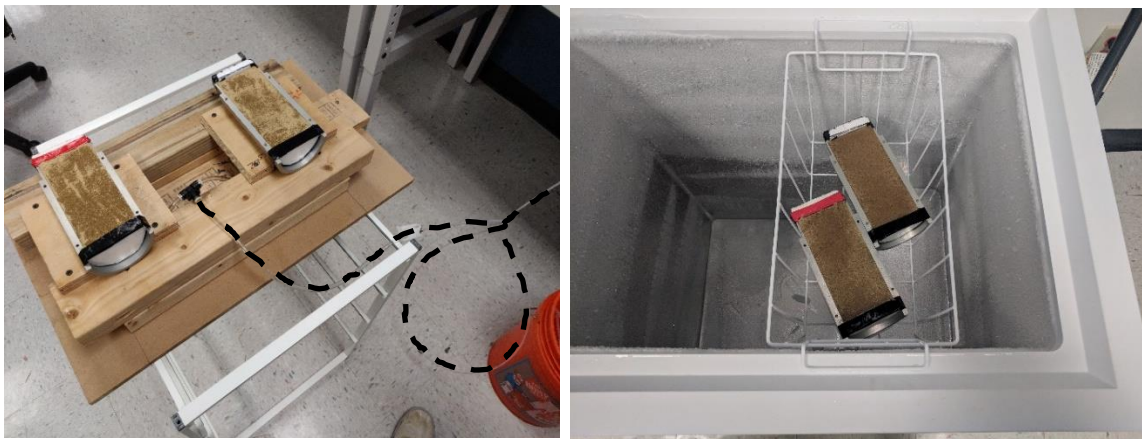

a) **b)**

Figure 6. (a) The vacuum line from the split mold is attached to the water line from the water panel and water is injected into the sand specimen until the sand resembles the split mold to the left. (b) Place the split molds in the freezer and leave it for 3 hours.

4. Take out the split molds from the freezer and remove the Styrofoam caps from the split molds. Use the palms of the hands to rub against the split molds to generate a small amount of heat in the split molds and push the sand specimen from the bottom of the split mold carefully. If the sand specimen is not budging, use the palm of the hands and rub against the bottom of the split mold to generate more heat so it allows the sand specimen to come out as shown in Figure 7a. This process may take 1-5 minutes depending on how much the sand has frozen.

   After the sand specimen is removed, quickly place the two halves against each other and push it into a latex membrane that has been wrapped and vacuumed around a 2.8 in membrane stretcher given in Figure 7b.

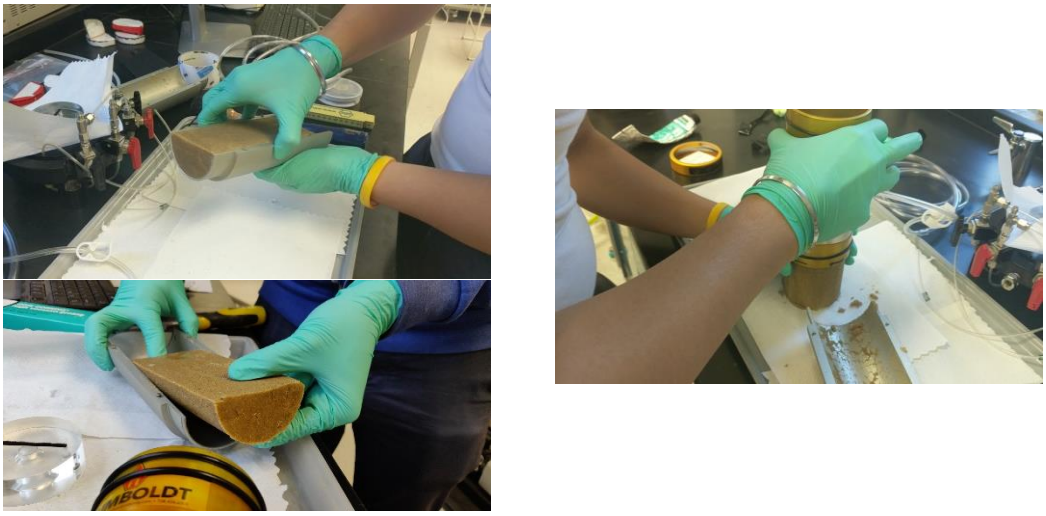

a) **b)**

Figure 7. a) Use the palm of the hands to rub against the split mold to increase the temperature of the mold enough that allow the sand specimen to be pushed out. b) Attach the two frozen pieces together and insert it inside the latex membrane wrapped around the membrane stretcher.

5. Place the frozen specimen on the bottom cap of the triaxial cell and unwrap the bottom half of the latex membrane and attach it with the O-rings from the membrane stretcher to the bottom cap as given in Figure 8a. Release the vacuum on the membrane stretcher and place the top cap on top of the frozen specimen, afterwards unwrap the top half of the membrane on the membrane stretcher and remove the membrane stretcher as shown in Figure 8b. Attach the O-ring on the top cap and insert the water lines into the specimen as shown in Figure 8c.

Measure the height and the diameter of the specimen before putting it inside the triaxial chamber.

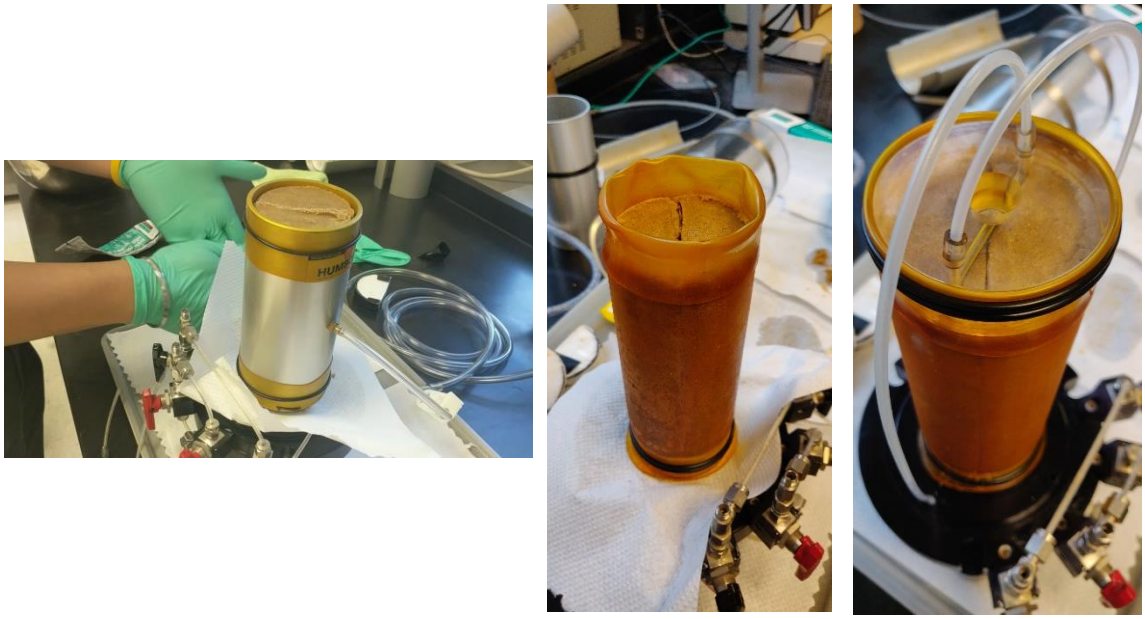

a) **b)** **c)**

Figure 8. a) The latex membrane is under vacuum from the membrane stretcher and the frozen specimen is placed on top of the bottom cap. b) Unwrap the bottom membrane and the top membrane and remove the membrane stretcher. c) Place the top cap and attach the O-rings to the specimen and insert the water lines.

Appendix C – Details of Sample Saturation

Vertical:

1. Prepare the vacuum pump (Figure 9) required for this section as the vacuum pressure will hold the sand specimen in place during the process of building the triaxial cell. Turn on the vacuum pump and attach the pipe to the bottom drainage lines (red knobs) and close of the top drainage line (black knobs) to create a vacuum within the sand specimen as shown in Figure 10a. Wait for 30 seconds to let the vacuum pressure circulate through the sand specimen. Start to remove the split mold by slowly removing the mold shell from the specimen as shown in Figure 10b. Measure the height and the diameter of the specimen while it is standing under the vacuum.

Figure 9. The vacuum pump used for holding the vertical sand specimen in place and used for removing water from the horizontal sand specimen.

a) **b)**

Figure 10. a) The vacuum pressure is placed on the sand specimen while the split mold being attached. b) Once the sand specimen is under vacuum for 30 seconds, remove the split mold and the sand specimen should stand by the vacuum pressure.

2. Once the sand specimen is able to stand with the pressure of the vacuum, remove any sand particles from the base of the triaxial cell and start to attach the O-ring for the base of the triaxial cell, the triaxial chamber, the piston with the O-ring attached to it and the triaxial tie rods to hold the triaxial cell in place. Use high vacuum grease on the triaxial chamber and cell to have water tight seal. Tighten the tie rods and insert the water line to the fill cell on the water panel to the triaxial cell as shown in Figure 11.

Figure 11. Create the triaxial chamber while specimen is under vacuum and tighten the tie rods to secure the chamber.

Remember to attach a tube line to the piston when filling the cell with water, otherwise there will be a buildup of pressure in the cell. Fill the cell with the water and remove any air bubbles within the chamber by slightly tilting the chamber to the tube line to allow the air bubbles to be removed. Zero the cell

pressure transducer from the computer and attach the transducer on the top of the piston as shown in Figure 12.

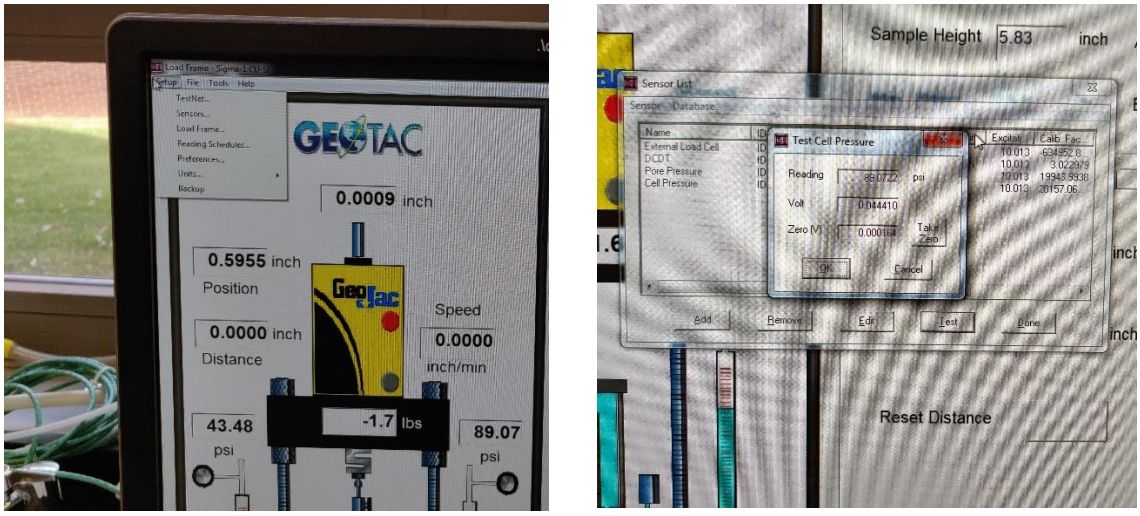

(a) **(b)**

Figure 12. (a) First click on Setup and go to Sensors. (b) Then click on Cell Pressure and then Test. After that Take Zero and press Ok.

After connecting the cell pressure transducer, close the bottom drainage valves (red knob) on the triaxial cell and shut off the vacuum pump. Take the water drainage line from the fill cell and attach it to position 3 on the water panel. Turn the knob on position 3 from vacuum to pressure and turn on position 3. Open the gage and increase the pressure in the cell slowly to 3 psi while opening the bottom drainage (red knob) valve to release the vacuum pressure.

3. Move to the CO_2 process by attaching the CO_2 tank to the bottom drainage valves and attach an open water line to the top drainage valve into a flask filled with water to create a bubble chamber. Open CO_2 tank by turning the silver knob twice, then turn the black knob on the pressure gauge clockwise and then turn the blue knob on the pressure gauge clockwise slowly until the pressure reading on the gauge is 1.5 – 2 psi and open the bottom and top drainage valves to let the gas flow through to the bubble chamber as shown in Figure 13.

(a) **(b)**

Figure 13. (a) Connect the CO_2 line to the bottom drainage valves and connect an open water line to the top drainage valves and connect that to (b) a bubble chamber.

Perform this process for 20 minutes with a constant pressure. After the CO_2 process is completed, turn off the CO_2 by turning the blue knob counter-clockwise, turning the black knob on the CO_2 pressure gauge off and turning the silver knob on the CO_2 tank counter-clockwise to shut it off. Close the bottom and top drainage valves to stop the CO_2 from escaping the sand specimen.

4. Attach a water line from position 1 on the water panel to the bottom drainage valves in the triaxial cell. Put the burette in position 1 of the water panel into pressure, keep the burette on the “both” position, and turn “on” position 1. Open the bottom and top drainage valves and let the deaired water percolate through the sand specimen without any back pressure. Perform this process until the burette reads 24 ml and switch position 1 to the “off” position. Take out the water line from position 1 and place it into position 2 and repeat the same process done in position 1. Once the water starts to come out of the top drainage line, close off one top drainage valves and let all the air bubbles come out until there is only water coming out. Do the same process for the other top drainage valve until water is coming out. Turn the bottom and top drainage valves off and remove the open water line from the top drainage valve.
5. Close off position 2 and refill the burettes in both position 1 by turning the knob from “pressure” to “vacuum” and turning the knob slowly from “off” to “tank” and fill the burette in position 1 to 0.5 ml on the burette. Perform the same task on the burette in position 2 and fill it with deaired water. Zero the pore pressure transducer from the computer the same way in Figure 12 and attach the pore pressure transducer to the top drainage valve of the triaxial cell. Keep the water line attached to position 2 and the bottom drainage valves, turn the knob from “vacuum” to “pressure”, open the “gage” and slowly turn the pressure knob to 2 psi and close the “gage”. Open the “gage” in position 3 and turn the pressure knob to 5 psi and close the “gage”. Finally open the “gage” in position 2 and increase

the pressure to 3 psi and close the “gage”. Leave the sand specimen overnight to saturate completely for best results otherwise leave it for 2-3 hours. Use an Allen key to open the screw slightly on the cell and pore pressure transducer to let the water saturate the device. Open the transducer a small amount until water droplets start to come out and then tighten the screws once that is completed.

6. After the specimen has rested, perform the Skempton’s B-value check by going to the computer, clicking on the tools tab, then click on B-value check and click on start as shown in Figure 14.

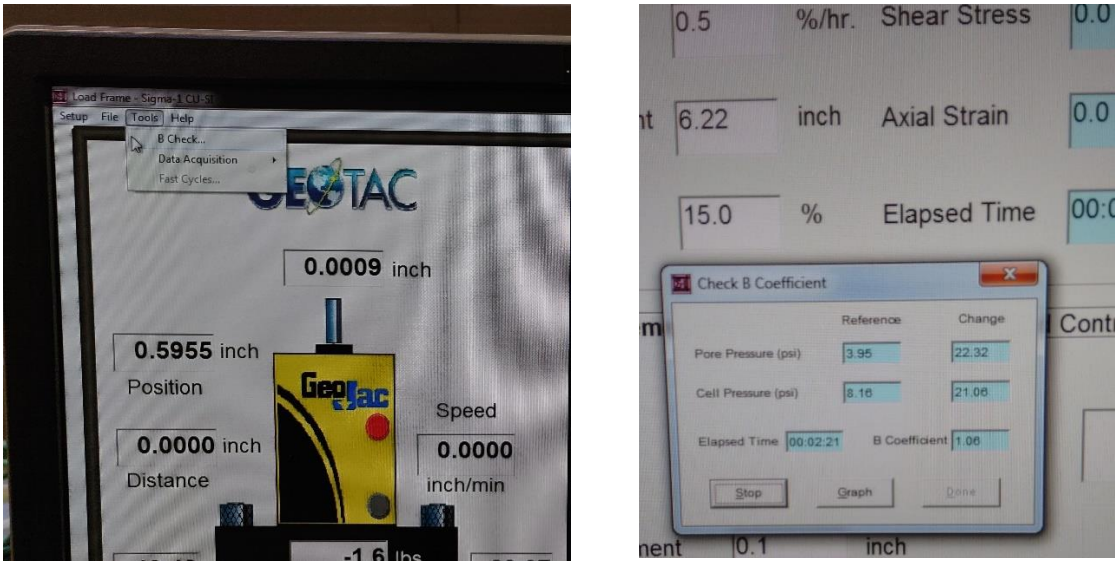

(a) **(b)**

Figure 14. (a) Open tools and click on B check. (b) Press “Start” once the B-check opens.

Close off the bottom drainage valves and the burette in position 2 and 3. Open the "gage" to position 3 and increase the pressure by 10 psi. Close the "gage" and turn "on" position 3. Let the B-check on the computer run for a minute and record the B-coefficient. The B-coefficient value should be between 0.95-0.99. Once that value is reached, open the "gage" in position 3 and slowly decrease the pressure to 5 psi then close the "gage". Turn on position 2 once you have reached 5 psi in position 3.

Horizontal:

1. Once the sand specimen is in place, record the diameter and the height of the specimen and build the triaxial chamber as done in the vertical sand specimen without using the vacuum pump. After the chamber has been built, insert the water line into the "fill cell" and the triaxial cell. Fill the triaxial cell with water and remove any air bubbles from the cell as done in the vertical specimen. Attach the water line from the "fill cell" to position 3 and attach the cell pressure transducer to the triaxial chamber. Close the bottom and top drainage valves and open the "gage" to position 3 and increase the pressure in the cell to 3 psi.
2. Attach an open water line to the top drainage valve and open the bottom and top drainage valves. Have an empty bowl at the end of the top drainage valve to collect the water and introduce warm water through the bottom drainage valves by injecting through a water injection as indicated in Figure 15.

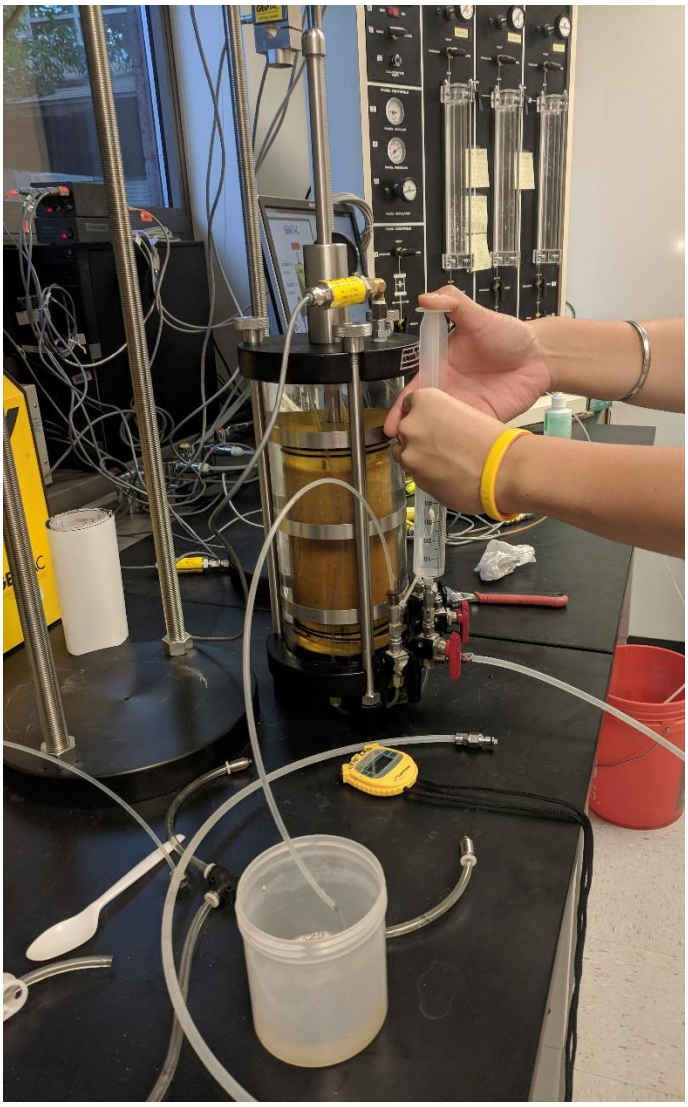

Figure 15. Inject water into the bottom drainage valve and cold water exits from the top drainage valve.

Keep injecting warm water into the bottom of the drainage valves until the water coming out of the top drainage valve reaches 22°C. After the temperature is reached, close all the drainage valves and attach the vacuum pump to a sump

catcher and attach the sump catcher to the bottom drainage valve in the triaxial cell. Turn on the vacuum pump and open all the drainage valves, and remove all the water from the sand specimen as shown in Figure 16.

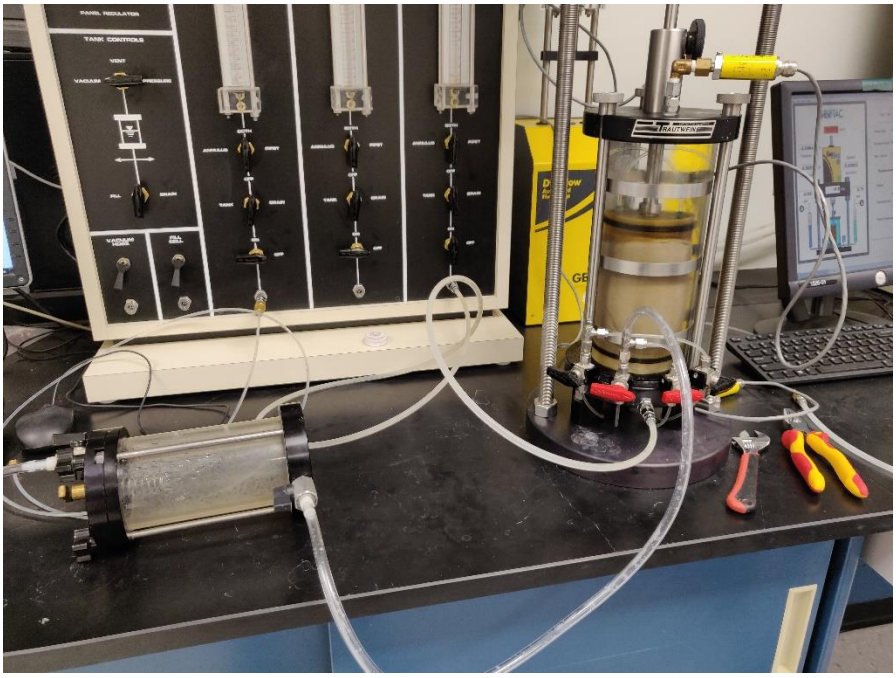

Figure 16. Vacuum pump connected to the sump that collects water which is then connected to the bottom drainage valves to suck in the water.

3. After the water has been drained from the specimen, turn off the vacuum and remove the vacuum. From here, perform the same steps as done for the vertical sand specimen in step 3 for introducing CO_2 into the specimen. Let the CO_2 percolate through the sand specimen for 30 minutes instead of 20 minutes as this is a wetter sand sample. Follow steps 4-6 in the vertical specimen to saturate the

sand specimen and measure the B-check of the specimen. The B-check value should be in the range of 0.93-0.98.

Appendix D – Details of Isotropic Compression

The steps to isotropic compression are the same for the vertical and horizontal sand specimens. To perform the isotropic compression test, increase the pore pressure to 4.7 psi by in position 2. Have a difference of 0.3 psi between the pore pressure and the confining pressure. After that, turn "off" the burette in position 2 and turn the knob from "both" to "pipette". Reduce the water in the pipette by turning the knob slowly from "off" to "drain" and reduce the water level to 10 ml and bring it back to "off". Turn "on" the burette for position 2. Make a table as given in Table 1 to record the isotropic compression values.

Table 1. An example table used to record the values for the isotropic compression test.

	0.6 psi	0.9 psi	1.2 psi	1.7 psi	2.0 psi	2.3 psi	2.6 psi	2.9 psi
0 sec								
5 sec								
10 sec								
20 sec								
30 sec								
1 min								
2 min								

The isotropic compression will be performed under 3 different compressions; 20, 60, and 180 kPa. Those pressures are 2.9, 8.7, and 26.1 psi respectively under the kPa to psi conversion. Similar to Table 1, make a table with different loading sequences for 8.7 and 26.1 psi to incrementally increase the confining pressure in the cell.

After the table is made, turn to the water panel and turn "off" the confining pressure which is position 3 and open the "gage". Increase the pressure by an incremental amount and close the gage. Start the timer when position 3 is turned "on" and start recording the values. Perform this step until the confining pressure for the sand specimen has been reached.

Appendix E – Details of Drained Shearing

1. Once the sand specimen has been confined to the said pressures, move to triaxial shearing. Unlock the piston in the triaxial chamber while holding onto the piston itself and touch the top cap of the specimen by pushing the piston rod down and lock the piston in place once you have touched it. Place the triaxial chamber underneath the GeoJac and lower the loading cell in the GeoJac by the computer. Move the mouse to the double arrow button and click it, then press the "start" button and the loading cell will start to lower itself. If the speed of the loading cell is too fast, press "stop" and click on the single arrow button and press "start" which will all the loading cell will move slowly. Move the loading cell till the piston and the loading cell are barely touching each other and double check the correctness by looking at the weight the loading cell is putting on the piston. The weight on the piston from the loading cell should be 0 lbs or below coming from

the computer. Once that is completed, zero the DCDT and the loading cell before beginning the test, and this process is the same as Figure 12 but click on “External Load Cell” and “DCDT”.

2. The next task is to enter the “Specimen Data” for the test that is going to be running. For this, go to setup and click on “Specimen Data”. Enter the project number and the height and diameter of the specimen that will be running and save this file in a folder or on the desktop. Next, enter the “Test Data” by going into setup and clicking on “Test Data”. Enter the strain rate for the sand tests as 10 %/hour, keep the maximum strain at 20%, loading type is compression, and click on “Perform Unload/ Reload Cycles” when performing an unloading/ reloading test. The number of cycles that will run is going to be 1, the strain at which the specimen will unload will be the strain rate right after the maximum failure point, the creep time will be 0 minutes and reload the specimen after the specimen has unloaded after 1% axial strain. For example, if the specimen reaches maximum failure at 6% axial strain, the sample will be unloaded at 7% axial strain and it will be reloaded at 6% axial strain. After entering the test data, click “Ok” and move to the water panel.
3. If the test is being perform on loose sand specimens, turn “off” position 2, turn the know to “pipet”, turn from “pressure” to “vacuum” and turn the bottom knob from “off” to “tank”. Increase the water to 3 ml, afterwards, move the knob from “tank” to “off”, then turn the knob from “vacuum” to “pressure”, and turn “on” position 2. Turn “off” position 3, turn the knob from “both” to “pipet”, then turn

the knob from “pressure” to “vent”, and then turn the knob from “off” to “drain”. Allow the water to drain till the water reaches 20 ml, afterwards, turn the knob from “drain” to “off”, “vent” to “pressure”, and turn “on” position 3.

4. If the sand specimen is dense or medium-dense, turn “off” position 2 and move the knob from “pipet” to “off” to “annulus”. Bring the water level in the annulus to 2 ml by draining the water (turn the knob to “vent” and “drain”) or adding the water (turn the knob to “vacuum” and “tank”). After that, bring position 2 back to “pressure” and turn “on” position 2. Move to position 3 and turn “off” the burette, turn the knob to “annulus”, then turn from “pressure” to “vent” and then turn the knob from “off” to “drain”. Drain the water to 20 ml in the annulus for position 3 and turn it “off”, then move from “vent” to “pressure” and turn “on” position 3.
5. Move to the computer, make sure all of the transducers are giving correct reading, double check the loading cell and the DCDT are zeroed, and make sure position 2 and position 3 are turned “on”. Finally make a table similar to Table 2 below to record the raw data that will be collected for the volumetric strain during the test. Once all of the preparations are done, move the mouse on the computer to “Start Test” and it will ask to unlock the piston. Unlock the piston and click “Ok”, wait for the piston to adjust and once the timer on the computer starts, start the stopwatch to start taking volume readings.

Table 2. Record the data in a table like this.

Time	Axial Strain (%)	Position 2 Reading (Calibration Factor of Annulus)	Position 3 Reading (Calibration Factor of Annulus)
0	0.00	3.0 or 2.0	20.0
10 sec			
20 sec			
30 sec			
40 sec			
50 sec			
1 min			
1 min 30 sec			
2 min			
2 min 30 sec			
3 min			
4 min			
5 min			
10 min			

6. To remove the triaxial chamber after testing, lock the piston, click on the up double arrows on the computer and press “start”. Move to position 2, open “gage”, turn the pressure knob to 0 psi, close “gage”, turn the knob from “pipet” or “annulus” to “both” and turn off position 2. Turn the knob on position 2 from “pressure” to “vacuum” and then “off” to “tank” and refill the burette with water until 0.5 ml. Perform the same procedure on position 3 and then remove the water lines and transducer from the triaxial cell. The triaxial chamber is ready for dismantling.

Appendix F – Details of Processing Raw Test Results

Isotropic compression:

The first set of results that need to be measured is the isotropic compression results where the volumetric strains increase with the addition of incremental increases in pressure. Table 3 indicates the values that need to be calculated after the data is recorded from the isotropic compression tests. Produce a similar table as given in Table 3 to calculate the values for the specimens under 60 kPa and 180 kPa.

Table 3. To record raw isotropic compression results and calculate the volumetric strain.

	Confining Pres. (psi) (σ_3)	**Confining Pres. (kPa) (σ_3)**	**Vol. (ml) (V)**	**Vol. change (ΔV)**	**V_O (cm^3)**	**Vol. Strain (ε_{vol} %)**
1	0.3	2.0				
2	0.6	4.1				
3	0.9	6.2				
4	1.2	8.3				
5	1.7	11.7				
6	2.0	13.8				
7	2.3	15.9				
8	2.6	17.9				
9	2.9	20.0				

Record the volume (V) when the confining pressure of the specimen is incrementally increased during isotropic compression. The volume is measured from the pipet during the increase in confining pressure. Calculate the volume change (ΔV) in the specimen by using Equation 2.

Equation 2 $$(V_n - V_1) * -1 = \Delta V$$

V_n are the different volumes measured in the burette and it is subtracted by the V_1, which is the value measured during the start of the isotropic compression test. V_o is the volume of the specimen that is measured before the start of the isotropic compression test. Using Equation 3, measure the volumetric strain (ε_{vol} %) of the specimen.

Equation 3 $$\left(\frac{\Delta V}{V_o}\right) * 100\% = \varepsilon_{vol}\%$$

Graph the volumetric strain results against the confining pressure in kPa given in Figure 17.

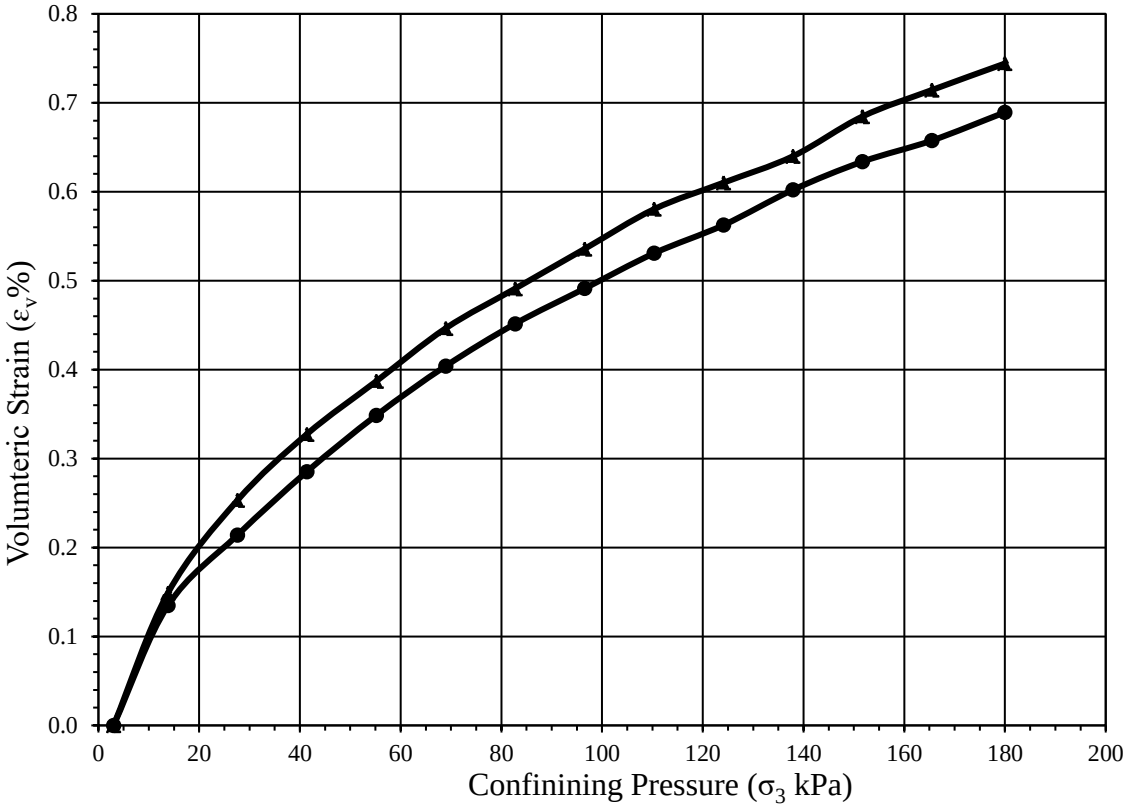

Figure 17. Graph the incremental increases in the volumetric strain as the confining pressure increases.

The volumetric strain of the specimen should therefore increase as the confining pressure is incrementally increased within the triaxial chamber.

Stress-strain plot:

After the completion of the shear test, locate the specimen data file that was saved at the start of the test and this will either be saved on a folder that was created or on the desktop under a TRX file. Within the computer, locate an excel file under the name of

"Template for CU" and open that file. Once the file has opened, the excel file will be under the "Results 1" tab. Click on "Import File", and that shall open a screen that asks to import the test file. This test file will be the specimen data as a TRX file, click on that file and press "Open". It will open another screen once the file has been imported and that will be to save the file which should be saved under a specific folder with a file name. After the file is saved, then a small box will appear asking to save as a macro-free workbook, click "yes" to that box. Go to the "Results 1" tab once that procedure is complete and click on "Calculate" on the "Results 1" excel sheet. This will in turn calculate and enter all of the data that was measured during the testing of the specimen. With the calculated results, create two columns in the "Results 1" tab as "Sigma 1-Sigma 3 (psi)" and "Sigma 1-Sigma 3 (kPa)". Under the "Sigma 1-Sigma 3 (psi)" column, calculate the difference between sigma 1 (psi) versus sigma 3 (psi) during the test. Convert the "Sigma 1-Sigma 3 (psi)" values into kPa and calculate it in the "Sigma 1-Sigma 3 (kPa)" column.

Create a XY scatter graph with lines in a new tab and name the tab as "Sigma 1-Sigma 3", within that graph, create a plot for axial strain (ε_1) versus "Sigma 1-Sigma 3 (kPa)" where the plot should similar to Figure 18.

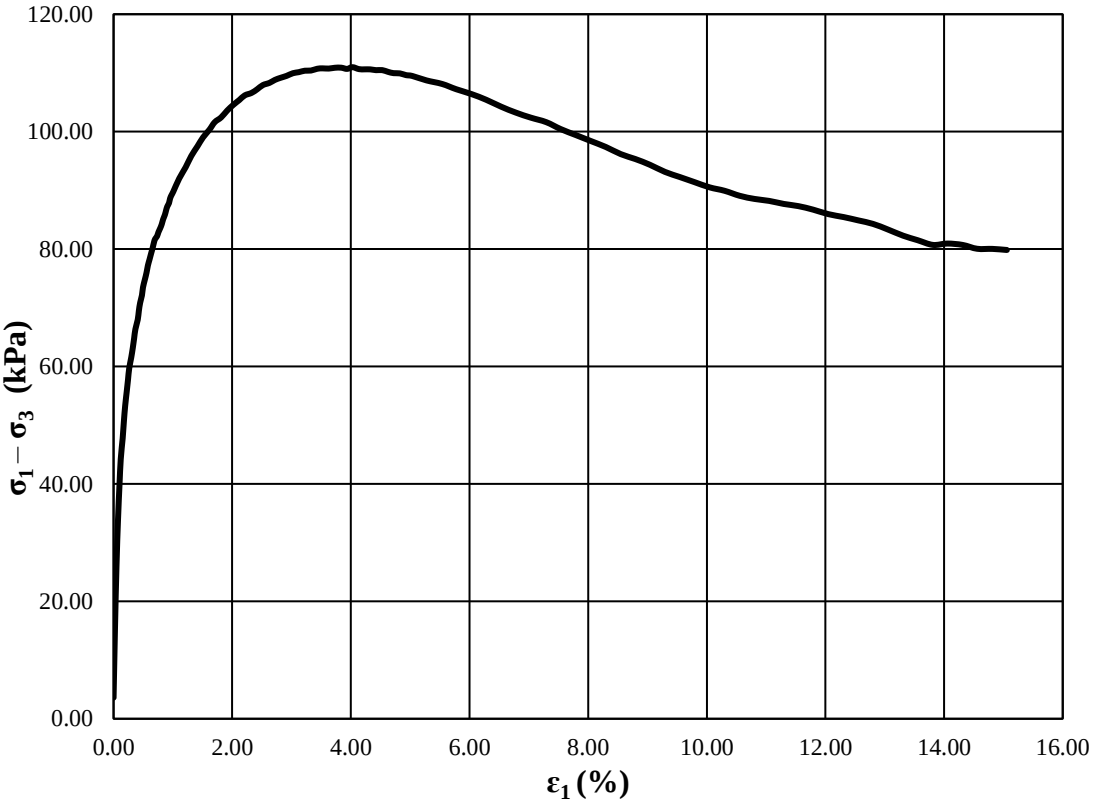

Figure 18. Create this graph with the data collected for the axial strain and sigma 1-sigma 3.

Volumetric Results:

Create a new tab within the same excel sheet that has the stress-strain plot with the name “volume change” and create a table similar to Table 4.

Table 4. Table to log the volume readings from the specimen under testing.

Time (min)	Vol. reading	ΔV value without calibration	ΔV calibrated	Vol. of Specimen (V_O)	$\Delta V/V_O$	Axial Strain (ε_1)
0						
0.17						
0.3						
0.5						
0.67						
0.83						
1						

Record the volume readings that were taken during the testing and calculate the ΔV as given in Equation 2. After calculating the ΔV, multiply the ΔV values with the calibration factor if the test was performed under an annulus burette in the "ΔV calibrated" column. Record the original volume of the specimen before the start of the test and calculate the $\Delta V/V_O$ in the "$\Delta V/V_O$" column. Use the ΔV that has been calibrated during the calculation of $\Delta V/V_O$ for tests that were performed in an annulus. Insert the axial strain (ε_1) values in the axial strain column that was taken during testing. Create another tab with a XY graph and plot an axial strain (ε_1) vs $\Delta V/V_O$ graph as shown and change the y-axis in the reverse order as shown in Figure 19.

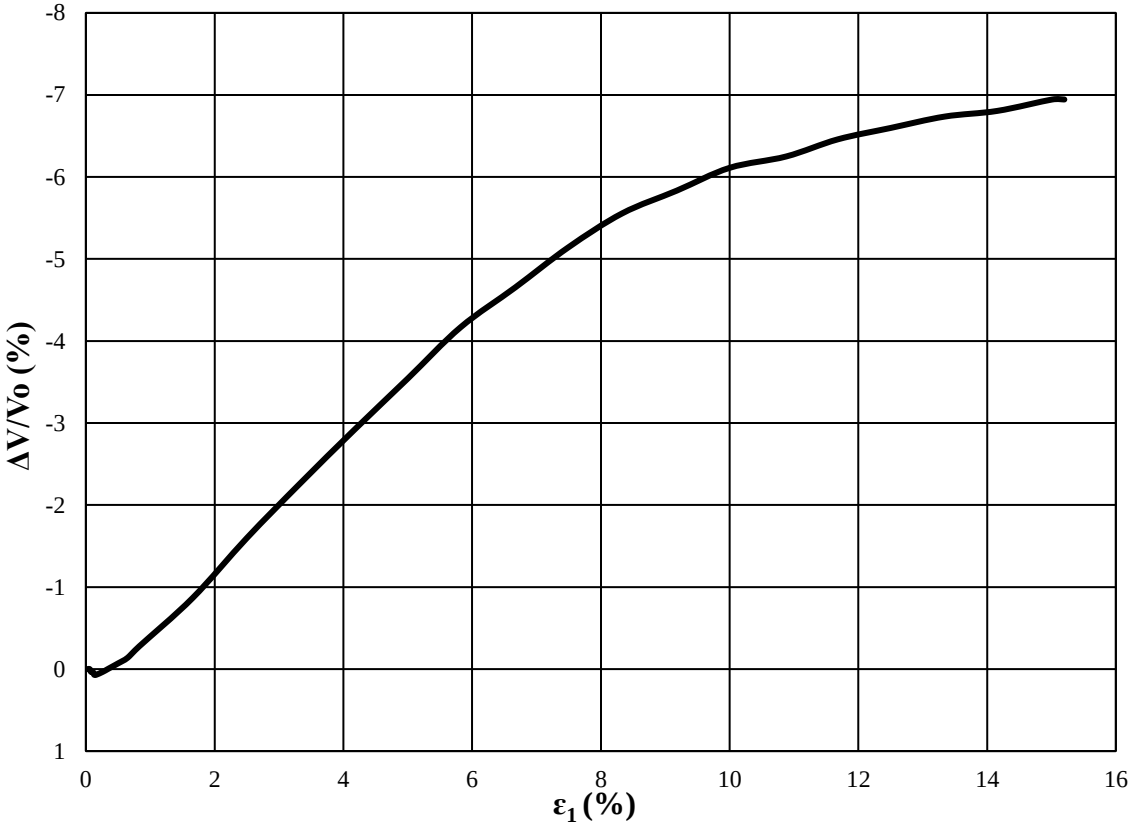

Figure 19. Volumetric Strain graph with the y-axis switched to the reverse order.

Friction Angles:

Open the "Results 1" tab and highlight the row with highest obliquity value that is measured during testing. From the highest obliquity, calculate the friction angle of the specimen with Equation 4.

Equation 4

$$\arcsin \frac{(Obliquity(\frac{\sigma_1}{\sigma_3}) - 1)}{(Obliquity(\frac{\sigma_1}{\sigma_3}) + 1)}$$

Use equation 4 to measure the friction angle for all of the tests under different loading conditions.

Dilation Angle:

Measure the angle of the curve on the $\Delta V/V_O$ graph and draw a tangent on the curve and use Pythagoras theorem as shown in. The line of the tangent is taken from the axial strain of the peak shear failure for the specimen and use that axial strain to draw the line of tangent to measure the angle of the curve as shown in Figure 20 for medium dense sand .

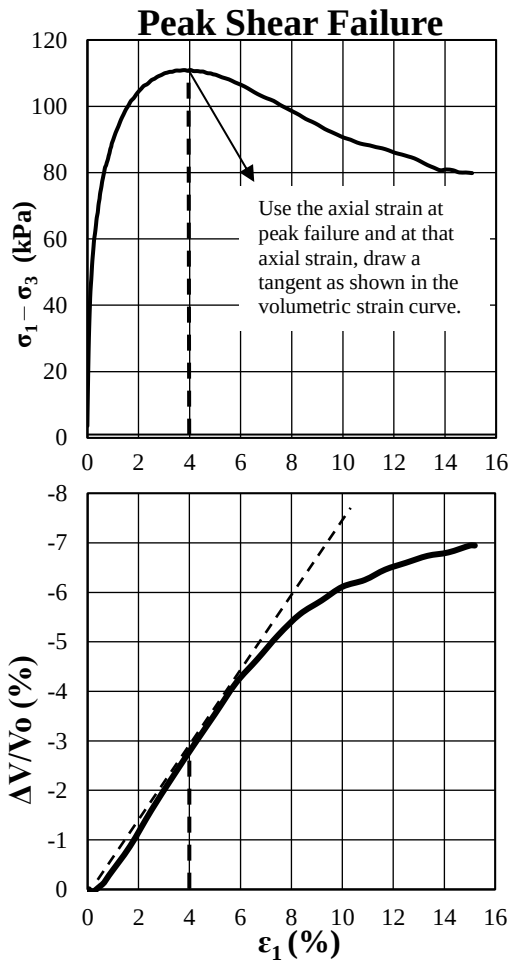

Figure 20. Create a tangent to get an angle of curve on the $\Delta V/V_O$ graph.

After measuring the angle of the curve, create a table in excel as shown in Table 5 to calculate the dilation angle of each angle of curve that was measured.

Table 5. Use to calculate the dilation angle from the angle of curve

Angle of Curve	Dilation Angle (ψ)	Ψ*PI()/180 = u	Sin(u) = v	v*2 = w
		Eq. 5	**Eq. 6**	**Eq. 7**
1-v = x	w/x = y	Atan(y) = z	z/PI()*180 = p	Angle of Curve – p
Eq. 8	**Eq. 9**	**Eq. 10**	**Eq. 11**	**Eq. 12**

In this method, insert the angle of curve measured from the volume change graph in the "Angle of Curve" column. After that enter a dilation angle (ψ) in the "Dilation Angle" column and use the trial and error method to reach the correct dilation angle when the "Angle of Curve – p" equals 0. Use this method on excel and formulate the equations in Table 5 and insert different variations of dilation angles till the correct one is achieved.

Appendix G – Parameters for the Soil Hardening Model

Table 6 gives all of the parameters calculated for the single hardening model for the vertical and horizontal conditions in the sand. All the parameters were calculated using the formulations from Lade et. al in, "Single hardening constitutive model for frictional materials" I, II, and III and from Niels Trads in, "Experimental study and modeling of the mechanical behavior of cross-anisotropic sandstone." These papers have the formulations to calculate the necessary parameters from the isotropic compression and triaxial test

results performed within this paper. Below are the steps to calculate the 5 components of the Single Hardening Model (SHM).

1. Failure Parameter:

   Table 6 given below describes the values that are needed to calculate the failure parameter.

Table 6. Parameters needed to calculate I_1, I_3, Y and X axis values.

Input	
psi to P_a =	0.07

Test	e (Void Ratio)	σ_3' (psi)	σ_1' (psi)	σ_3' (atm)	σ_1' (atm)	I_1	I_3	Y	X
PS-33	0.803	2.97	13.24	0.20	0.90	1.30	0.04	33.48	0.767
PS-34	0.821	2.94	12.51	0.20	0.85	1.25	0.03	30.52	0.799

The void ratio is pre-calculated during specimen measurements. The σ_3' and σ_1' values are taken from the Sigma 3 and Sigma 1 column in the "Results tab" of the triaxial compression data. The maximum Sigma 3 and Sigma 1 values should be taken for calculating the failure parameters. Convert σ_3' and σ_1' values from psi to atm (atmosphere). Calculate the I_1 and I_3 values with equations 5 and 6 which will be used to calculate the X and Y axis values given in equations 7 and 8.

Eq. 5 $$I_1 = \sigma_1' + (2 * \sigma_3')$$

Eq. 6 $$I_3 = \sigma_1' * \left(\sigma_3'^2\right)$$

Eq. 7 $$\text{Y (axis)} = I_1^3 / I_3$$

Eq. 8 $$\text{X (axis)} = 1 / I_1$$

Calculate the X and Y axis values and put them into a X Y scatter graph detailing with the X axis values in the X-axis and the Y axis values in the Y-axis. The x-axis and the y-axis on the graph should be in logarithmic scale and draw a power trendline on the scattered plots as shown in figure 21.

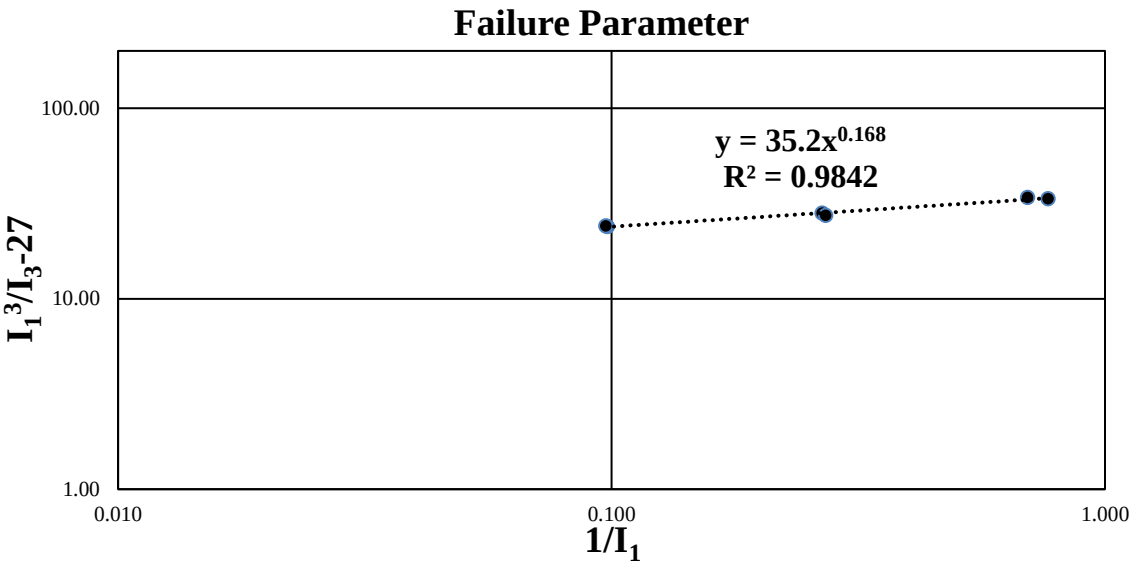

Figure 21. Graph the X and Y values as shown above and get the failure parameters.

2. Elastic Parameter:

   For calculating the elastic parameters, use the triaxial compression results calculated for the unloaded and reloaded sand specimens. Use table 7 to calculate the values for graphing the elastic parameters.

Table 7: Write down all of the raw results and calculate the X and Y axis values.

Input			Subparameter							
psi to P_a =	0.07		R =	95.35227						
v =	0.45									
Test	**e (Void Ratio)**	**σ_3' (psi)**	**σ_1' (psi)**	**E**	**σ_3' (atm)**	**σ_1' (atm)**	**I_1**	**J_2'**	**Y**	**X**
PS-35	0.801	3.066	13.445	42.412	0.209	0.915	1.332	0.166	42.412	17.631
PS-35	0.801	2.885	2.699	9.914	0.196	0.184	0.576	0.000	9.914	0.337
PS-36	0.789	3.075	13.368	123.110	0.209	0.910	1.328	0.164	123.110	17.357
PS-36	0.789	2.892	2.718	11.134	0.197	0.185	0.579	0.000	11.134	0.339

Similar to the failure parameter, σ_3' and σ_1' are taken from the Sigma 3 and Sigma 1 column. Two σ_3' and σ_1' values will be taken, which means the point when the specimen is starts the unloading process and one when the specimen is starts the reloading process. Write them the same way as shown in table 7 and calculate the next set of equations.

Eq. 8 $$E = \Delta(\sigma_1 - \sigma_3)/\Delta\varepsilon_1$$

Eq. 9 $$I_1 = \sigma_1' + (2 * \sigma_3')$$

Eq. 10 $$J_2' = \frac{1}{6} * ((\sigma_1' - \sigma_3')^2 + (\sigma_3' - \sigma_1')^2)$$

Eq. 11 $$v = 1 - \frac{\Delta\left(\frac{\Delta V}{V_O}\right)}{\Delta\varepsilon_1}$$

Eq. 12 $$R = 6 * \frac{(1+v)}{(1-2v)}$$

Eq. 13

$$Y(axis) = \frac{E}{p_a}$$

Eq. 14

$$X(axis) = \left(\frac{I_1}{P_a}\right)^2 + R * \frac{J_2'}{p_a^2}$$

Calculate the Young's modulus (E) by taking the difference between the ($\sigma_1 - \sigma_3$) and dividing that by the difference of the axial strain. This difference given in figure 22 shows that the difference is a tangent that needs to be calculated.

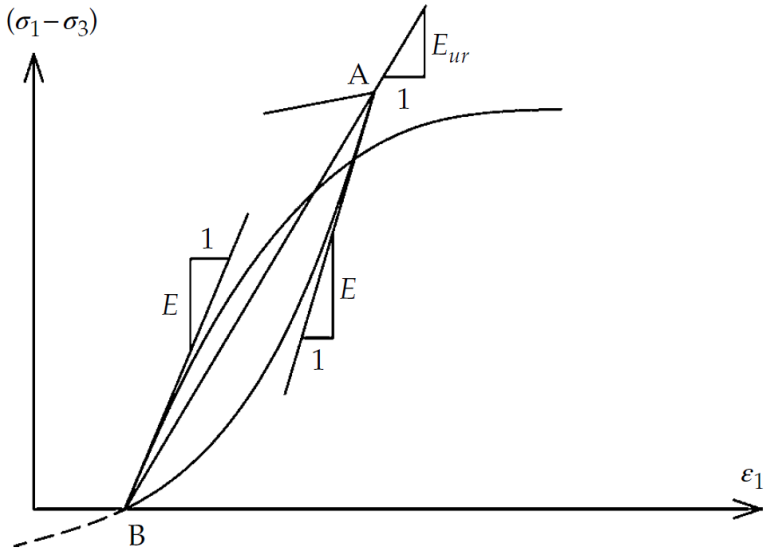

Figure 22. The calculation of Young's modulus done when the tangent of the line is taken during unloading and during reloading.

Convert the σ_3' and σ_1' from psi to atm and calculate the equations from 8 to 10. For equations 9 and 10, calculate the Poisson's ratio from the volumetric strain graph of when the specimen reloads. During the process of reloading, the

specimen will push water out which is moment when the Possion's ratio is captured as shown in figure 23.

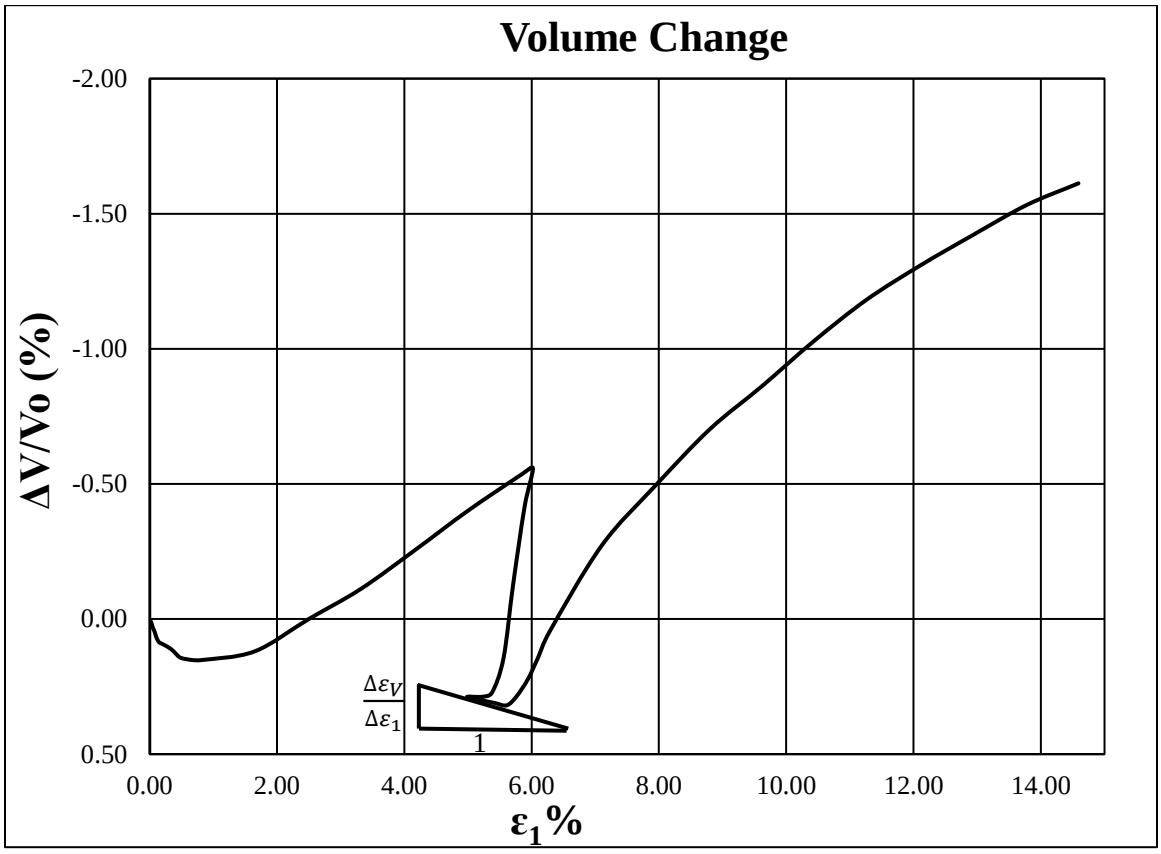

Figure 23. During the reloading process, measure the Poisson's ratio for every test

Once that is completed, calculate all of the Poisson's ratio values from the other unloaded-reloaded tests and take the average value from them. Use that value to calculate the R value within the specimen and calculate the X and Y axis values. Draw the figure similar to the failure parameter and measure the trend line within the graph to get the elastic parameters. The graph should be in logarithmic scale for both x and y-axis and the trend line should be a power trendline.

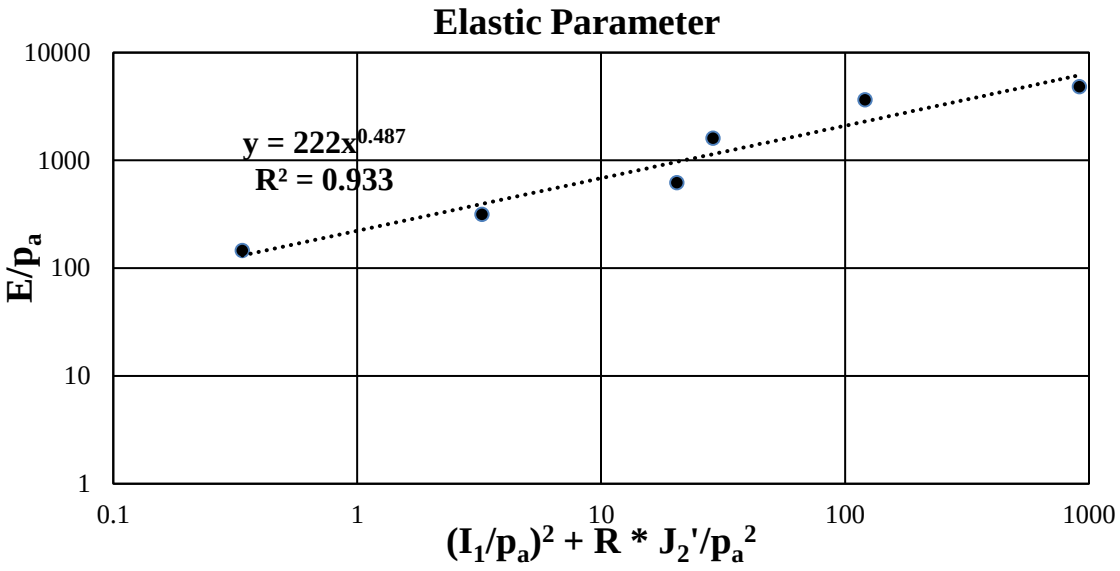

Figure 23. The X and Y values should be put into a XY scatter plot and the trend line will give the elastic parameters.

3. Hardening Parameters:

   The same process is undertaken for isotropic compression as done in appendix F.

   Use table 3 and attach table 8 to calculate the isotropic compression values.

Table 8. Attach the four columns to table 3.

σ_3/p_a	ε_{vol}	$\Delta W_{Total}/p_a$	W_{Total}/p_a

Given are the equations needed to calculate the hardening parameters needed from the isotropic compression data.

Eq. 15

$$\frac{\sigma_3}{p_a}$$

Eq. 16 $$\varepsilon_{vol} = \varepsilon_{vol\%} * 100$$

Eq. 17 $$\frac{\Delta W_{Total}}{p_a} = \frac{\frac{\sigma_{3,n1}}{p_a} + \frac{\sigma_{3,n2}}{p_a}}{2 * (\Delta\varepsilon_{vol})}$$

Eq. 18 $$\frac{W_{Total}}{p_a} = \frac{\Delta W_{Total,1}}{p_a}, \frac{W_{Total}}{p_a} = \frac{W_{Total,1}}{p_a} + \frac{\Delta W_{Total,2}}{p_a}$$

Eq. 19 $$\frac{I_1}{p_a} = 3 * \frac{\sigma_3}{p_a}$$

The addition of the four columns will be calculated with the isotropic compression values that were calculated. For equation 17, the $\frac{\sigma_{3,n1}}{p_a} + \frac{\sigma_{3,n2}}{p_a}$ means the same thing as $\Delta\frac{\sigma_3}{p_a}$ except instead of a minus sign, put an addition sign. Equation 18 is slightly different where the first $\frac{\Delta W_{Total,1}}{pa}$ equals $\frac{W_{Total}}{p_a}$ but every point after that is the previous $\frac{W_{Total}}{p_a}$ value plus the next $\frac{\Delta W_{Total}}{p_a}$ value. After that, graph the $\frac{I_1}{p_a}$ values against the $\frac{W_{Total}}{p_a}$ values on a logarithmic scale and place a power trendline to show the hardening parameters as given in figure 24.

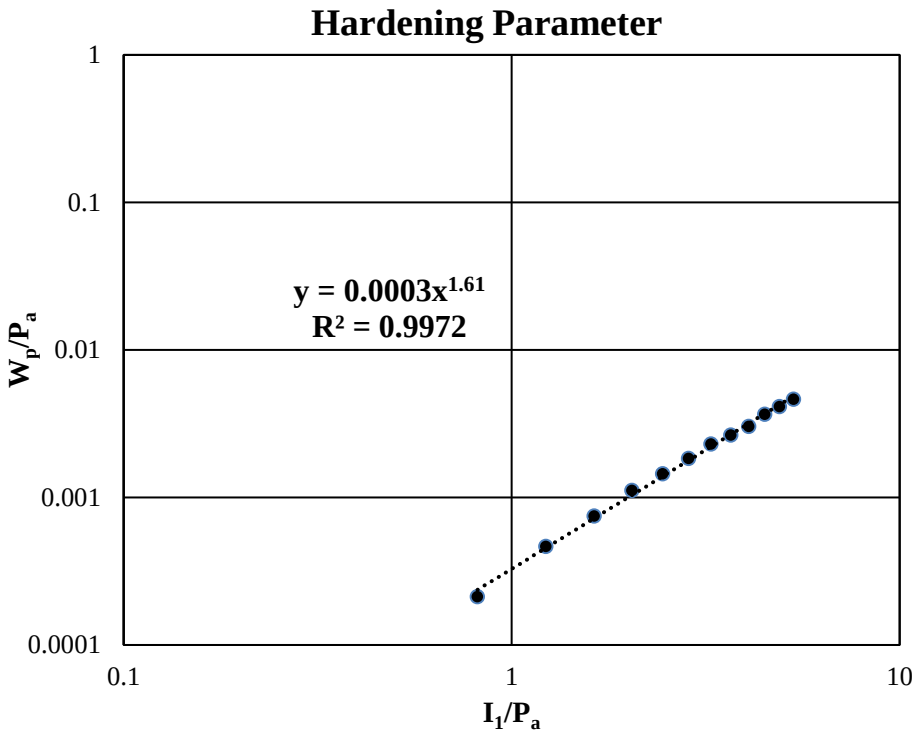

Figure 24. Draw the hardening parameter graph to get the parameters from the trendline.

4. Plastic Potential and Yield Criterion:

   The plastic potential and yield criterion are to be calculated in tandem as both sets of parameters utilize the same sets of data. Table 9 describes the data that is needed for calculating the parameters.

Table 9. The data need to calculate the plastic potential and yield criterion.

X_{ix}	X_{iy}	Q	S	h
18.137	4.641	0.452	0.724	1.359
19.147	4.826	0.817	0.811	0.920

The equations used to calculate the data needed in table 9 will utilize Sigma 1 and Sigma 3 where those values need to be converted into atmosphere.

Eq. 20
$$\psi = \frac{0.00155}{m^{1.27}}$$

Eq. 21
$$X_{ix} = \frac{1}{1+\nu_p}\left[\frac{I_1^3}{I_2^2}\left(\sigma_1+\sigma_3+2\nu_p\sigma_3\right)+\psi_1\frac{I_1^4}{I_3^2}\left(\sigma_1\sigma_3+\nu_p\sigma_3^2\right)\right]-3\psi\frac{I_1^3}{I_3}+2\frac{I_1^2}{I_2}$$

Eq. 22
$$X_{iy} = \psi_1\left(\frac{I_1^3}{I_3}\right)-\left(\frac{I_1^2}{I_2}\right)$$

Eq. 23
$$h = \log\frac{\left(\psi_1 \bullet \frac{I_{1\_B}^3}{I_{3B}}-\frac{I_{1\_B}^2}{I_{2B}}\right)\bullet e}{27\psi_1+3} / \log\frac{I_{1A}}{I_{1B}}$$

Eq. 24
$$I_2 = -(2\sigma_1'\sigma_3'+\sigma_3'\sigma_3')$$

Eq. 25
$$Q = \ln\frac{\left(\frac{W_p}{D\bullet p_a}\right)^{\frac{1}{\rho}}}{\left(\psi_1\bullet\frac{I_1^3}{I_3}-\frac{I_1^2}{I_2}\right)\left(\frac{I_1}{p_a}\right)^h}$$

Eq. 26
$$S = \frac{1}{\eta_1}\bullet\left(\frac{I_1^3}{I_3}-27\right)\left(\frac{I_1}{p_a}\right)^m$$

Equation 20 utilizes the value ‘m’ that comes from the failure parameter. Equation 21 is the x-axis formula needed to be calculated for the plastic potential value. The formula will utilize the stress invariants and sigma 1 and sigma 3

values from the test results captured from previous calculations. X_{iy} is the y-axis that is capture for the plastic potential and it utilizes the same values captured from previous tests. The 'h' formula will use the stress invariants that are previously calculated and use equation 24 to calculate the second stress invariant. Equation 25 utilizes W_p which comes from hardening parameter and equation 26 has η_1 which comes from the failure parameter. The plastic potential function is drawn on a linear scaled graph and the trend is a linear trend line as shown in figure 25. Once the trendline is capture use the formulas in the graphs to calculate the plastic potential values.

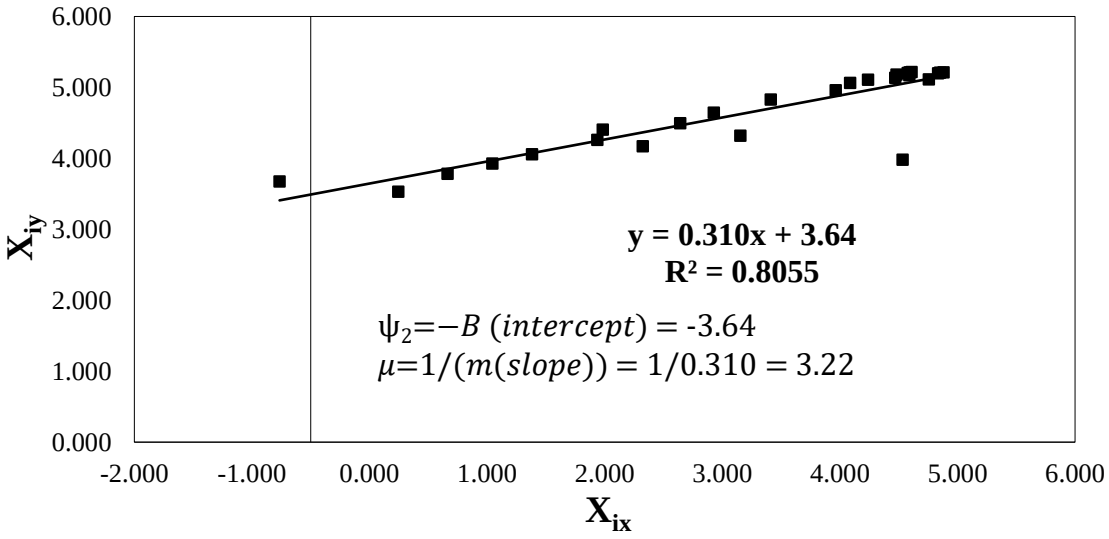

Figure 25. Plastic potential graph used to measure the ψ_2 and μ functions.

The last parameter needed is the ‘α’ parameter which can be captured by graphing the Q values versus the S values shown in figure 26.

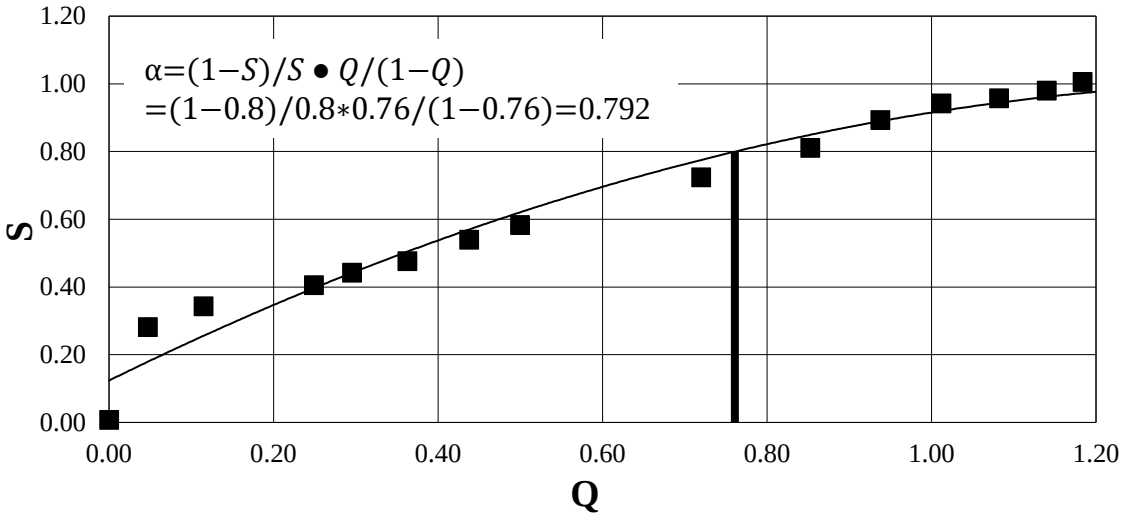

Figure 26. Use the Q versus S figure to calculate the alpha value parameter

Measure the ‘h’ for each σ_1 and σ_3 value in a given triaxial test and highlight the ‘h’ value that has the highest $\sigma_1 - \sigma_3$ value and that value will be the final parameter needed to calculate the single hardening model. Table 6 shows the values that have been previously calculated for horizontal and vertical sand specimens using the same methods as shown in appendix G.

Table 10. All the calculated parameters of the Single Hardening Model for sand in the vertical and horizontal direction.

Tests by Siddharath Singh								
Source of the sand	Commericial Hardware Store							
Description of sand	Playsand							
Void Ratio	0.79	0.79	0.80	0.65	0.65	0.59	0.60	0.60
Relative Density	34%	34%	31%	76%	76%	93%	92%	92%
Angularity	Sub-angular to Sub-Rounded							
Mineralogy	Consists of mostly quartz							
Confining Pressure	20, 60, 180 kPa							
Gradation	Medium to Fine Sand Poorly Graded							
Density	Vertical Loose Set-1	Vertical Loose Set-2	Horizontal Loose	Vertical Medium Dense	Horizontal Medium Dense	Vertical Dense	Horizontal Dense Set 1	Horizontal Dense Set 2
Elastic Properties:								
ν (Poissons Ratio)	0.46	0.45	0.42	0.38	0.37	0.35	0.34	0.33
M (Elastic Component)	223	224	258	607	531	676	539	550
λ (Elastic Exponent)	0.49	0.49	0.43	0.50	0.38	0.43	0.43	0.38
Failure Criterion:								
a (Offset due to cohesion)	0.00	0.00	0.00	0.00	0.00	0.00	0.00	0
m (Failure exponent)	0.17	0.14	0.12	0.21	0.20	0.23	0.18	0.14
η_1 (Opening Angle)	35	33	30	67	49	81	54	50
Hardening Function:								
C (Plastic Work Constant)	0.00037	0.00035	0.00039	0.00033	0.00034	0.00030	0.00032	0.00032
p (Hardening Exponent)	1.77	1.79	1.66	1.68	1.62	1.57	1.68	1.62
Plastic Potential:								
Y_2	-3.35	-3.41	-3.49	-3.45	-3.26	-3.33	-3.35	-3.45
m	2.45	2.42	2.21	2.44	2.20	2.46	2.28	2.36
Yield Parameter								
h	0.68	0.68	2.21	0.84	0.67	0.71	0.75	0.75
a	0.92	1.03	2.52	0.25	4.70	0.28	1.82	0.70

Appendix H – Location of Copies of Files Used in this Research

1) Locations for all the raw shear test results are kept inside the journal article folder, data, and compartmentalized in the horizontal or vertical folder.
2) All the Single Hardening Model data and parameters are kept inside journal article, data, and compartmentalized in the SHM folder.
3) All of the friction and dilation angle data is kept inside the journal article folder, data, and inside the friction and dilation angles folder.

4) Inside the data folder are other excel files in relation to the gradation, overall parameters and initial data measurements of the tests performed.
5) The installation to SciLab is kept inside journal article and then the data folder. Follow the steps during the installation process.
6) Relevant literature in regards to the SHM is kept inside the journal article folder, data, and inside the literature to SHM folder.

Appendix I – Dilation Angle

Dilation angles come from the phenomenon of dilatancy in granular material where granular materials are subjected to shear deformations and volume change within granular specimens. The density of the granular materials will dictate the amount of dilation that will occur within a given specimen such that dense sand specimens will have a higher amount of volume expansion as compared to loose sand specimens. Therefore, dilation has an effect of increasing the friction angle above the true value as given in equation 27.

Eq. 27 $$\Phi = \Phi' + \psi$$
Eq. 28 $$\Phi' = \Phi - \psi$$

Equation 28 takes the effective friction angle by subtracting the friction angle from the dilation angle to equal the effective friction angle of the granular specimen. As shown in figure 27, the horizontal blocks slide over one another on a flat plane indicating that there is shearing taking place at a constant volume where no dilation occurs. However, in the sawtooth model, the sawtooth teeth are sliding on a rough plane at an angle ψ with the

same friction angle. That is when the volume of changes causing dilation within the specimen to increase.

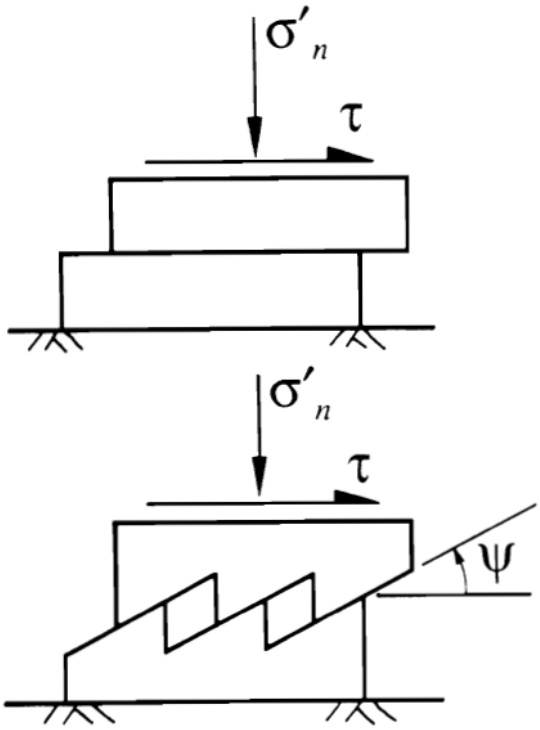

Figure 27: This a sawtooth model describing the how dilatancy is achieved in soils. (Houlsby, 1991)

Due to the dilatancy, the angle of friction increases as the confinement increases till the specimen reaches peak strength value. It is after the specimen has reached peaked strength value that the angle of friction within the specimen decreases quickly. This cause

slopes, tunnels, piles, and footings to have major decreases in soil strength after it reaches its peak strength values.

Appendix J – Cross Anisotropy versus Anisotropy

To understand anisotropy and cross-anisotropy, the definition of isotropy is needed to be understood. Isotropy as a general definition means the uniformity in all orientations. Therefore, the definition of isotropy of soils and granular materials is the soil consisting of perfectly shaped grains or particles, with flow rates being the same in all the directions and various other factors would be equal. Anisotropy however is the opposite of isotropy in definition where the property is directionally dependent. In the case of soil and granular properties, the shape of the grains is not consistently perfect, the flow rates would be different and there would other various factors that would not be equal. Anisotropy is separated into two different forms, inherent anisotropy which is particle assembly in its virgin state before a loading occurs and induced anisotropy which is the results of the strains associated with the applied stress. The particle assembly for inherent anisotropy are performed during vertical deposition process for granular material which creates horizontal bedding planes that forms the of cross-anisotropy within soils. The horizontal bedding planes dictate the cross-anisotropy that is within soils that have inherent anisotropy.

Appendix K – Membrane Penetration Effect

Membrane penetration effect is the “penetration of the rubber membrane enclosing the triaxial specimen into the voids between the particles of the granular soils.” (Lade, 2016) This causes volume change within the triaxial test with changing confining

pressures, due to this, an experimental error is created since the measured volume change is not solely representative of the soil skeleton compression, but it is also representative of the volume of water that is forced out by the penetrating membrane. “The magnitude of the membrane penetration effect is dependent on the average particle size, the magnitude and change in the confining pressure, the modulus and the thickness of the rubber membrane, and the surface area the membrane covers.” (Lade, 2016) Frydman et al. (1973) described that membrane penetration is negligible for particles that have an average particle sizes below 0.1-0.2 mm. However, membrane penetration decreases as the confining pressure within the cell increases and that is due to particle crushing. Due to this, multiple methods are utilized to either minimize or eliminate membrane penetration that occurs within triaxial compression cells.

Membrane penetration can be minimized by increasing the specimen diameter, increasing the membrane thickness, and using a stiffer membrane. For case of Play sand that is used within these tests, increasing the membrane thickness would minimize the membrane penetration instead of increasing the specimen diameter as the membrane can be modified slightly to produce better results. Kiekbusch and Schuppener (1977) and Lo et al. (1989) modified the flexural characteristics of the membrane to limit the degree of penetration where in both studies, the inside of the membrane was coated with a layer of liquid latex and rubber before deposition of the soil. In this study we had the option to use two different membrane thicknesses which included 0.012 inches and 0.025 inches. The focus of this study was not to quantify the membrane effect and therefore the thicker membrane was used for the experiments. However in the future study, a comparison of

the results from the two different membrane thicknesses maybe conducted. Based on the observations, potentially, it maybe decided that with the thicker membrane, Play sand can be tested without creating the specific grain size distribution that was implemented in this study.

The effect of particle size on membrane penetration is also compared by Baldi and Nova (1984), Frydman et al. (1973) and Nicholson et al. (1993a) and each version tested different variations of particles measuring different levels of membrane penetration. From a mean grain size of 0.01 – 0.1 mm, the normalized membrane penetration is negligible, from 0.1 – 1 mm mean grain size, the penetration increases and from 1 – 10 mm mean grain size, the membrane penetration is significantly high. Nicholson et al. (1993a) used fines in the granular material and measure if the fines reduced the membrane in the granular soils. The results were the same for the specimen between 0.01-0.1 mm in mean grain size, however from 0.1 – 1 mm mean grain size, the membrane penetration effect was negligible. Particle size after 1 – 10 mm particle size showed an increase in the membrane penetration. From Nicholson et al. (1993a) findings, granular material can be tested from the field if it is within the 0.1 – 1 mm range of particle size as the membrane penetration is negligible. In the case for Play sand that is used, the grain size distribution shows that the sand on its own can be tested in the triaxial compression test without sieving the material as most of the sand fits of the particle size where membrane penetration is negligible.

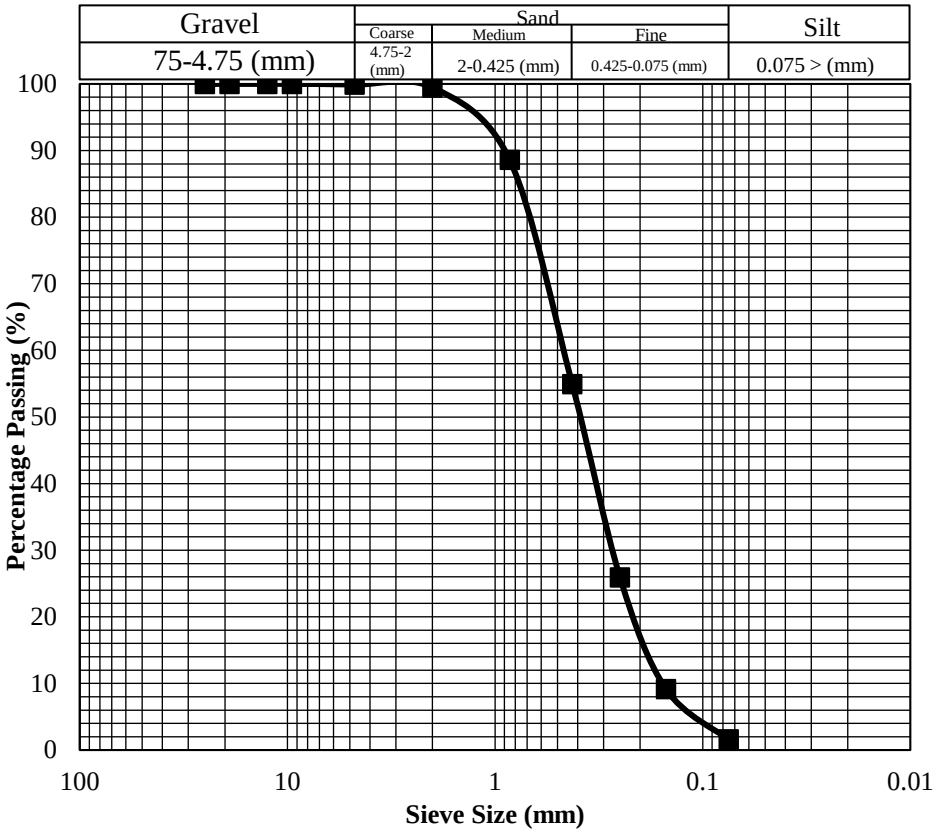

Figure 28. Grain size distribution of Play sand before sieved between #40 (0.425 mm) and #200 (0.075 mm) sieves.

Appendix L – Definitions

Principal stress: The stress that is the normal stress acting on the principal plane.

Principal plane: The plane in which the shear stress is zero and the plane on which it attains its maximum and minimum normal stress values.

σ_1: The maximum value of the principal stress is known as the Major Principal Stress (σ_1).

σ_2: The intermediate or the middle value of the principal stress is known as the Intermediate Principal Stress (σ_2) located between σ_1 and σ_3.

σ_3: The minimum value of the principal stress is known as the Minor Principal Stress (σ_3).

REFERENCES

Abelev, A. V., and Lade, P. V. 2003. Effects of Cross Anisotropy on Three-Dimensional Behavior of Sand. I: Stress–Strain Behavior and Shear Banding. Journal of Engineering Mechanics, ASCE, **129**(2): 160–166. https://doi.org/10.1061/(ASCE)0733-9399(2003)129:2(160)

Abelev, A.V., and Lade, P.V. 2004. Characterization of Failure in Cross-Anisotropic Soils. Journal of Engineering Mechanics, ASCE, **130**(5): 599-606

.

Abelev Andrei V., Gutta Suresh K., Lade Poul V., & Yamamuro Jerry A. (2007). Modeling Cross Anisotropy in Granular Materials. *Journal of Engineering Mechanics*, *133*(8), 919–932. https://doi.org/10.1061/(ASCE)0733-9399(2007)133:8(919)

Arthur, J. R. F., and Menzies, B. K. 1972. Inherent anisotropy in sand. Géotechnique, **22**(1): 115–128. https://doi.org/10.1680/geot.1972.22.1.115

Arthur, J.R.F., and Phillips, A.B. 1975. Homogeneous and Layered Sand in Triaxial Compression. Geotechnique, **25**(4): 799-815.

Baldi Gualtiero, & Nova Roberto. (1984). Membrane Penetration Effects in Triaxial Testing. *Journal of Geotechnical Engineering*, *110*(3), 403–420. https://doi.org/10.1061/(ASCE)0733-9410(1984)110:3(403)

Chairo, G., Kiyota, T. and Koseki, J. 2013. Strain localization characteristics of loose saturated Toyoura sand in undrained cyclic torsional shear tests with initial static shear. Soils and Foundations, **53**(1): 23-34.

El-Sohby, M. A., and Andrews, K. Z. 1973. Experimental examination of sand anisotropy. Proc., 8th Int. Conf. on Soil Mechanics and Foundation Engineering, Moscow, Soviet Union. **1:** 103–109.

S. Frydman, J. Zeitlen, and I. Alpan, "The Membrane Effect in Triaxial Testing of Granular Soils," *Journal of Testing and Evaluation* 1, no. 1 (1973): 37-41. https://doi.org/10.1520/JTE11599J

Haruyama, M. 1981. Anisotropic deformation-strength characteristics of an assembly of spherical particles under three dimensional stresses. Soils and Foundations, **21**(4): 41-55.

Hight, D.W., Gens, A. and Symes, M.J. 1983. The development of a new hollow cylinder apparatus for investigating the effects of principal stress rotation in soils, Geotechnique, **33(**4): 355-383.

Houlsby, G. (1991). How the dilatancy of soils affects their behavior. *Soil Mechanics Report Number 121/91*.

Janbu, N. 1963. Soil compressibility as determined by odometer and triaxial tests. Proc. European Conf. Soil Mechanics and Foundation Engineering, Wiesbaden, **1**: 19-25.

Kiekbusch, M., & Schuppener, B. (1977). Membrane Penetration and Its Effect on Pore Pressures. *Journal of the Geotechnical Engineering Division*, *103*(11), 1267–1279.

Lade, P.V. 2003. Analysis and Prediction of Shear Banding Under 3D Conditions in Granular Materials. Soils and Foundations. **43**(4): 161-172.

Lade, P.V. 2016. Triaxial Testing of Soils, Wiley, Chichester, U.K.

Lade, P.V. and Abelev, A.V. 2003. Effects of Cross-Anisotropy on three-dimensional behavior of sand. Part II: Volume Change behavior and failure. Journal of Engineering Mechanics, ASCE, **129**: 167-174.

Lade, P.V. and Abelev, A.V. (2005): Characterization of Cross-Anisotropic Soil Deposits from Isotropic Compression Tests. Soils and Foundations, **45**(5): 89-102.

Lade, P.V., and Duncan, J.M. 1973. Cubical triaxial tests on cohesionless soil. Journal of the Soil Mechanics and Foundations Division, ASCE, **99**(SM10): 793–812.

Lade, P.V., and Nelson, R.B. 1987. Modelling the Elastic Behaviour of Granular Materials. International Journal for Numerical and Analytical Methods in Geomechanics. **11**, 521-542. 10.1002/nag.1610110507

Lade, P., Liggio, C., and Yamamuro, J. 1998. Effects of Non-Plastic Fines on Minimum and Maximum Void Ratios of Sand. Geotechnical Testing Journal, ASTM **21**(4):336-347. https://doi.org/10.1520/GTJ11373J. ISSN 0149-6115

Lade, P.V., Rodriguez, N.M., and Van Dyck, E.J. 2014a. Effects of Principal Stress Directions on 3D Failure Conditions in Cross-Anisotropic Sand. Journal of Geotechnical and Geoenvironmental Engineering, ASCE, **140**(2): 04013001-1-12, DOI: 10.1061/(ASCE)GT.1943-5606.0001005

Lade, P.V., Van Dyck, E. and Rodriguez, N.M. 2014b. Shear banding in Torsion Shear Tests on Cross-Anisotropic Deposits of Fine Nevada Sand. Soils and Foundations, **54**(6): 1081-1093, DOI information: 10.1016/j.sandf.2014.11.004

Lade, P.V., and Wasif, U. 1988 Effects of Height-to-Diameter Ratio in Triaxial Specimens on the Behavior of Cross-Anisotropic Sand, *Advanced Triaxial Testing of Soil and Rock, ASTM STP 977,* ASTM, Philadelphia, 706-714.

Lam, W.K., and Tatsuoka, F. 1988. Triaxial compressive and extension strength of sand affected by strength anisotropy and sample slenderness. *Advanced Triaxial Testing of Soil and Rock,* ASTM STP 977, ASTM, Philadelphia, PA, 655-666.

Lee, K.L., and Seed, H.B. 1967. Drained strength characteristics of sands. Journal of Soil Mechanics and Foundations Division, ASCE, **93**(SM6): 117–141.

S. Lo, J. Chu, and I. Lee, "A Technique for Reducing Membrane Penetration and Bedding Errors," *Geotechnical Testing Journal* 12, no. 4 (1989): 311-316. https://doi.org/10.1520/GTJ10991J

Miura, K., Miura, S., and Toki, S. 1986. Deformation Behaviour of Anisotropic Dense Sand under Principal Stress Rotation, Soils and Foundations, **26(**1): 36-52.

Naughton, P.J., and O'Kelly, B.C. 2007. Stress non-uniformity in a hollow cylinder torsional sand specimen, Geomechanics and Geoengineering, **2**(2): 117-122.

Nicholson, P. G., Seed, R. B., & Anwar, H. A. (1993). Elimination of membrane compliance in undrained triaxial testing. I. Measurement and evaluation. *Canadian Geotechnical Journal*, *30*(5), 727–738. https://doi.org/10.1139/t93-065

Elimination of membrane compliance in undrained triaxial testing.II. Mitigation by injection compensation - Canadian Geotechnical Journal. (n.d.). Retrieved April 29, 2019, from https://www.nrcresearchpress.com/doi/abs/10.1139/t93-066#.XMdkhehKiUk

Oda, M. 1972a. Initial fabrics and their relations to mechanical properties of granular materials. Soils and Foundations, **12**(1): 17–36.

Oda, M. 1972b. The mechanism of fabric changes during compressional deformation of sand. Soils and Foundations, **12**(2): 1–18.

Oda, M. 1972c. Deformation mechanism of sand in triaxial compression tests. Soils and Foundations, **12**(4): 45–63.

Oda, M., Koishikawa, I., and Higuchi, T. 1978. Experimental study of anisotropic shear strength of sand by plane strain test. Soils and Foundations, **18**(1): 25–38.

O'Kelly, B., and Naughton, P. 2009. Study of Yielding of Sand under generalized Stress Conditions using a Versatile Hollow Cylinder Torsional Apparatus, Mechanics of Materials, **41**(3): 187-198.

Parkin, A.K., Gerrard, C.M., and Willoughby, D.R. 1968. Discussion on deformation of sand in shear. Journal of the Soil Mechanics and Foundations, ASCE, **94**(SM1): 336-340.

Powers, M. C., 1953. A New Roundness Scale for Sedimentary Particles. SEPM Journal of Sedimentary Research, **23**. https://doi.org/10.1306/D4269567-2B26-11D7-8648000102C1865D

Pradel, D., Ishihara, K., and Gutierrez, M. 1990 Yielding and Flow of Sand under Principal Stress Axes Rotation. Soils and Foundations, **30**(1): 87-99.

Rad, N.S. and Tumay, M.T. 1987. Factors affecting sand specimen preparation by raining. Geotechnical Testing Journal, ASTM, **10**(1): 31–37.

Raju, C.S. & Venkataramana, K. (1980). Undrained triaxial tests to assess liquefaction potential of sands - effect of membrane penetration.. Soils under cyclic and transient loading, volume 1. Proc. International symposium, Swansea 7-11 Jan. 1980. 483-494.

Rodriguez, N.M., and Lade, P.V. 2013. Effects of Principal Stress Directions and Mean Normal Stress on Failure Criterion for Cross-Anisotropic Sand, Journal of Engineering Mechanics, ASCE, **139**(11): 1592-1601.

Tatsuoka, F. Sakamoto, M., Kawamura, T., and Fukushima, S. 1986 Strength and Deformation Characteristics of Sand in Plane Strain Compression at Extremely Low Pressures. Soils and Foundations, **26**(1): 65-84.

Tokimatsu, K., & Nakamura, K. (1986). A Liquefaction Test Without Membrane Penetration Effects. *Soils And Foundations*, *26*(4), 127–138. https://doi.org/10.3208/sandf1972.26.4_127

Vaid, Y.P., and Negussey, D. 1984. Relative density of air and water pluviated sand. Soils and Foundations, **24**(2), 101–105.

Vaid, Y.P. and Negussey, D. 1988 Preparation of reconstituted sand specimens. In: *Advanced Triaxial Testing of Soil and Rock, ASTM STP 977* (eds R.T. Donaghe, R.C. Chaney, and M.L. Silver), pp. 405–417. ASTM, Philadelphia, PA.

Yamada, Y., and Ishihara, K. 1979. Anisotropic deformation characteristics of sand under three dimensional stress conditions. Soils and Foundations, **19**(2): 79-91.

BIOGRAPHY

Siddharath Singh graduated from Pathways World School, New Delhi, India, in 2011. He received his Bachelor of Science in Civil, Environmental, and Infrastructure Engineering from George Mason University in 2015. He started his Master of Science in Civil, Environmental, and Infrastructure from George Mason University in 2016.